AD-A085 579 SRI INTERNATIONAL MENLO PARK CA F/G 17/2.1
BINARY ERROR RATES FOR A TWO-COMPONENT SCINTILLATION CHANNEL.(U)
AUG 79 S C JOHNSON, C L RINO DNA001-77-C-0038
UNCLASSIFIED DNA-5071T NL

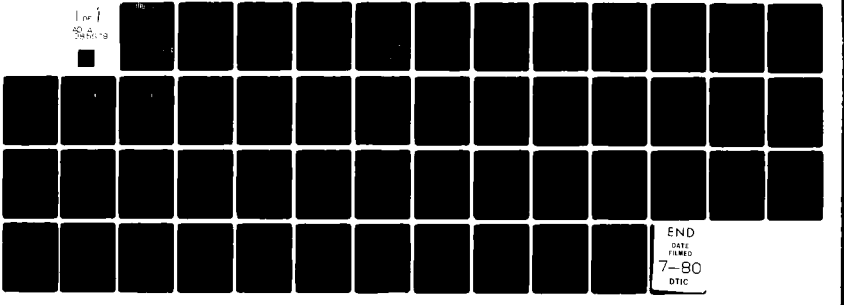

END
DATE FILMED
7-80
DTIC

DNA 5071T

BINARY ERROR RATES FOR A TWO-COMPONENT SCINTILLATION CHANNEL

Steven C. Johnson
Charles L. Rino
SRI International
333 Ravenswood Avenue
Menlo Park, California 94025

31 August 1979

Topical Report for Period 1 January 1979—31 August 1979

CONTRACT No. DNA 001-77-C-0038

APPROVED FOR PUBLIC RELEASE;
DISTRIBUTION UNLIMITED.

THIS WORK SPONSORED BY THE DEFENSE NUCLEAR AGENCY
UNDER RDT&E RMSS CODE B322078464 S99QAXHB05415 H2590D.

Prepared for
Director
DEFENSE NUCLEAR AGENCY
Washington, D. C. 20305

Destroy this report when it is no longer needed. Do not return to sender.

PLEASE NOTIFY THE DEFENSE NUCLEAR AGENCY, ATTN: STTI, WASHINGTON, D.C. 20305, IF YOUR ADDRESS IS INCORRECT, IF YOU WISH TO BE DELETED FROM THE DISTRIBUTION LIST, OR IF THE ADDRESSEE IS NO LONGER EMPLOYED BY YOUR ORGANIZATION.

UNCLASSIFIED

SECURITY CLASSIFICATION OF THIS PAGE (When Data Entered)

REPORT DOCUMENTATION PAGE		READ INSTRUCTIONS BEFORE COMPLETING FORM
1. REPORT NUMBER DNA 5071T	2. GOVT ACCESSION NO. AD-A085579	3. RECIPIENT'S CATALOG NUMBER
4. TITLE (and Subtitle) BINARY ERROR RATES FOR A TWO-COMPONENT SCINTILLATION CHANNEL		5. TYPE OF REPORT & PERIOD COVERED Topical Report for Period 1 Jan 79—31 Aug 79
		6. PERFORMING ORG. REPORT NUMBER SRI Project 5960
7. AUTHOR(s) Steven C. Johnson Charles L. Rino		8. CONTRACT OR GRANT NUMBER(s) DNA 001-77-C-0038
9. PERFORMING ORGANIZATION NAME AND ADDRESS SRI International 333 Ravenswood Avenue Menlo Park, California 94025		10. PROGRAM ELEMENT, PROJECT, TASK AREA & WORK UNIT NUMBERS Subtask S99QAXHB054-15
11. CONTROLLING OFFICE NAME AND ADDRESS Director Defense Nuclear Agency Washington, D.C. 20305		12. REPORT DATE 31 August 1979
		13. NUMBER OF PAGES 52
14. MONITORING AGENCY NAME & ADDRESS(if different from Controlling Office)		15. SECURITY CLASS (of this report) UNCLASSIFIED
		15a. DECLASSIFICATION/DOWNGRADING SCHEDULE

16. DISTRIBUTION STATEMENT (of this Report)

Approved for public release; distribution unlimited.

17. DISTRIBUTION STATEMENT (of the abstract entered in Block 20, if different from Report)

18. SUPPLEMENTARY NOTES

This work sponsored by the Defense Nuclear Agency under RDT&E RMSS Code B322078464 S99QAXHB05415 H2590D.

19. KEY WORDS (Continue on reverse side if necessary and identify by block number)

Scintillation
Channel Model
Error Rate
Binary Communication

20. ABSTRACT (Continue on reverse side if necessary and identify by block number)

This report describes a procedure for calculating the bit error rates for binary transmission through a two-component multiplicative channel of the type that has been proposed to represent the transionospheric channel. This procedure is then used to calculate the probability of error for several cases of interest that are not represented by commonly used Gaussian models. The non-Rician/Raleigh channel primarily affects the phase of the signal. Thus, the major impact is on coherent systems in a fast-fading environment.

DD FORM 1 JAN 73 1473 EDITION OF 1 NOV 65 IS OBSOLETE

UNCLASSIFIED

SECURITY CLASSIFICATION OF THIS PAGE (When Data Entered)

20. ABSTRACT (Continued)

In all cases, however, the effects of non-Rician and non-Gaussian fading are small when compared with a Rician or Gaussian channel with comparable fading levels.

CONTENTS

ILLUSTRATIONS

TABLES

I INTRODUCTION AND SUMMARY

Recent studies using the DNA Wideband satellite have indicated that the transionospheric radio channel is best represented by a two-component multiplicative model that separates received signal scintillations on the basis of their time structure (Fremouw et al., 1976, 1978).* This model appears to be useful from VHF to L-Band, and is sufficiently general that many simple channel representations (e.g., Rayleigh, Rician, log-normal) can be obtained as special cases. In this report we develop a general expression, applicable to a large class of binary diversity receivers, for the probability of bit error (P_e) using this channel. We then specialize this expression for noncoherent FSK and differentially-coherent phase-shift-keying (DPSK) communication systems, and examine the behavior of P_e as the scintillation parameters are varied. The expressions for P_e were evaluated numerically on a CDC 6400 computer; closed-form expressions for P_e could be obtained only in the simplest cases.

The results all tend to show that amplitude scintillation (fading) is by far the dominant factor in the determination of the error rate. Phase scintillation has some effect on DPSK if it is rapid, but it has virtually no effect on either FSK or DPSK if it is slow. In line with this, we found that, for reasonable parameter values, the focus component has relatively little effect on P_e, because it introduces primarily slow-phase scintillation. The addition of a coherent component to a scintillating signal reduces the error rate, of course, but significant reductions are not obtained until the coherent component contains more than one-half the total signal energy.

As with Rayleigh fading, rapid scintillation always increases the error rate. Rician and non-Rician models show essentially the same dependence on the fading rate (with one exception) as Rayleigh fading. The

*A list of references will be found at the end of the report.

exception occurs when most of the signal energy is in the quadrature term of the scatter component. Under these conditions, DPSK becomes much more sensitive to rapid scintillation than FSK.

Channel Model

The channel model proposed by Fremouw et al. (1976a,b) represents the complex received signal in the form

$$r(t) = r_s(t)\, r_f(t)s(t) + n(t) \quad , \tag{1}$$

where s(t) is the transmitted signal, n(t) is additive noise, and $r_s(t)$ and $r_f(t)$ are two statistically independent, complex stochastic processes having Gaussian and log-normal statistics respectively. In the transionospheric channel, $r_s(t)$ represents the diffractive scattering from small-scale irregularities and is referred to as the "scatter" component. The log-normal term, $r_f(t)$ represents the refractive focusing from large scale irregularities, and is referred to as the "focus" component. The correlation time for the scatter component is much smaller than the correlation time for $r_f(t)$; hence, the scatter term is associated with "fast fading," or rapid scintillation, and the focus term is associated with slow variations in the average amplitude and phase. A functional model for the channel consists of two cascaded multiplicative filters as shown in Figure 1.

The scatter component is given by

$$r_s(t) = \eta + h_s(t;f) \quad , \tag{2}$$

where η is a coherent or specular term, and

$$h_s(t;f) = x_s(t;f) + jy_s(t;f) \quad . \tag{3}$$

The quadrature terms $x_s(t;f)$ and $y_s(t;f)$ are zero-mean, stationary joint Gaussian processes with variances

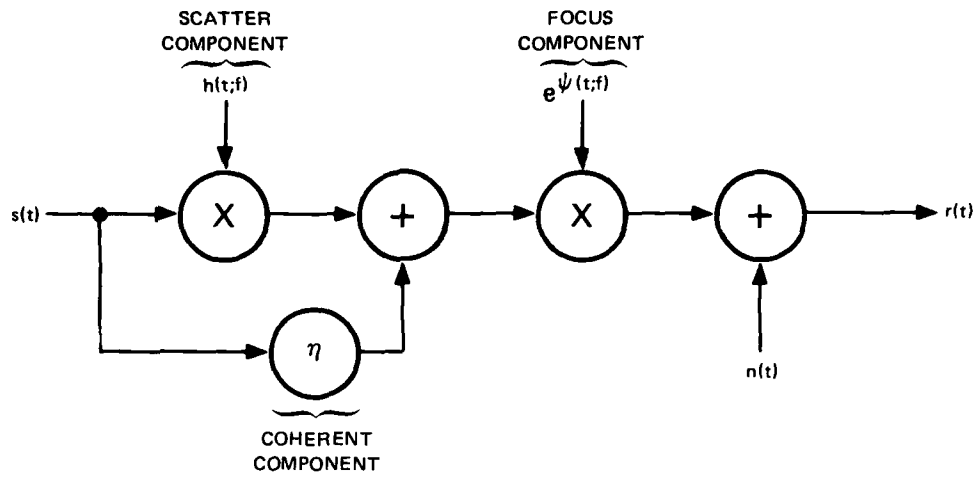

FIGURE 1 FUNCTIONAL DIAGRAM OF THE TWO-COMPONENT MULTIPLICATIVE CHANNEL

$$\overline{\left[x_s(t;f)\right]^2} = \sigma_x^2$$

$$\overline{\left[y_s(t;f)\right]^2} = \sigma_y^2 \quad , \tag{4}$$

and correlation coefficient, ρ_{xy}, given by

$$\rho_{xy} = \overline{x_s(t;f)\ y_s(t;f)}/\sigma_x\ \sigma_y \quad . \tag{5}$$

The overbar indicates the average (ensemble) of the quantity beneath. It is assumed that the functions involved are ergodic. The focus component is given by

$$r_f(t) = e^{\psi(t;f)} \quad , \tag{6}$$

where

$$\psi(t;f) = \chi(t;f) + j\phi(t;f) + \varepsilon \quad .$$

In Eq. (6), $\chi(t;f)$ and $\phi(t;f)$ are zero-mean stationary joint Gaussian processes with variances σ_χ^2 and σ_ϕ^2 and correlation coefficient $\rho_{\chi\phi}$.

We make the simplifying assumption that $h_s(t;f)$ and $\psi(t;f)$ are constant over the frequency band of interest, and shall henceforth drop the f variable from our notation. We also assume that the channel is lossless.

This imposes the constraints

$$\eta^2 + \overline{|h_s(t)|^2} = \eta^2 + \sigma_h^2 = 1 \quad , \tag{7}$$

where $\sigma_h^2 = \sigma_x^2 + \sigma_y^2$, and

$$\overline{|e^{\psi(t)}|^2} = 1 \quad . \tag{8}$$

It is straightforward to show that Eq. (8) implies that

$$\epsilon = -\overline{\chi^2} = -\sigma_\chi^2 \quad . \tag{9}$$

Seven parameters are required to characterize this channel:

- σ_x^2, σ_y^2 and ρ_{xy} are the variances and correlation coefficient of the scatter component,
- σ_χ^2, σ_ϕ^2 and $\rho_{\chi\phi}$ are the variances and correlation coefficient of the focus component, and
- τ is the correlation time of the scatter component.

The coherent intensity η^2 can be determined from (7). The properties of the scatter and focus components are such that $\sigma_\chi^2 \ll \sigma_\phi^2$, and the correlation time of the focus component is much larger than that of the scatter component. Thus, for the bit error rate computations only τ need be specified.

A typical example of a signal undergoing weak scintillation is shown in Figure 2. The scatter and focus components are shown separately in

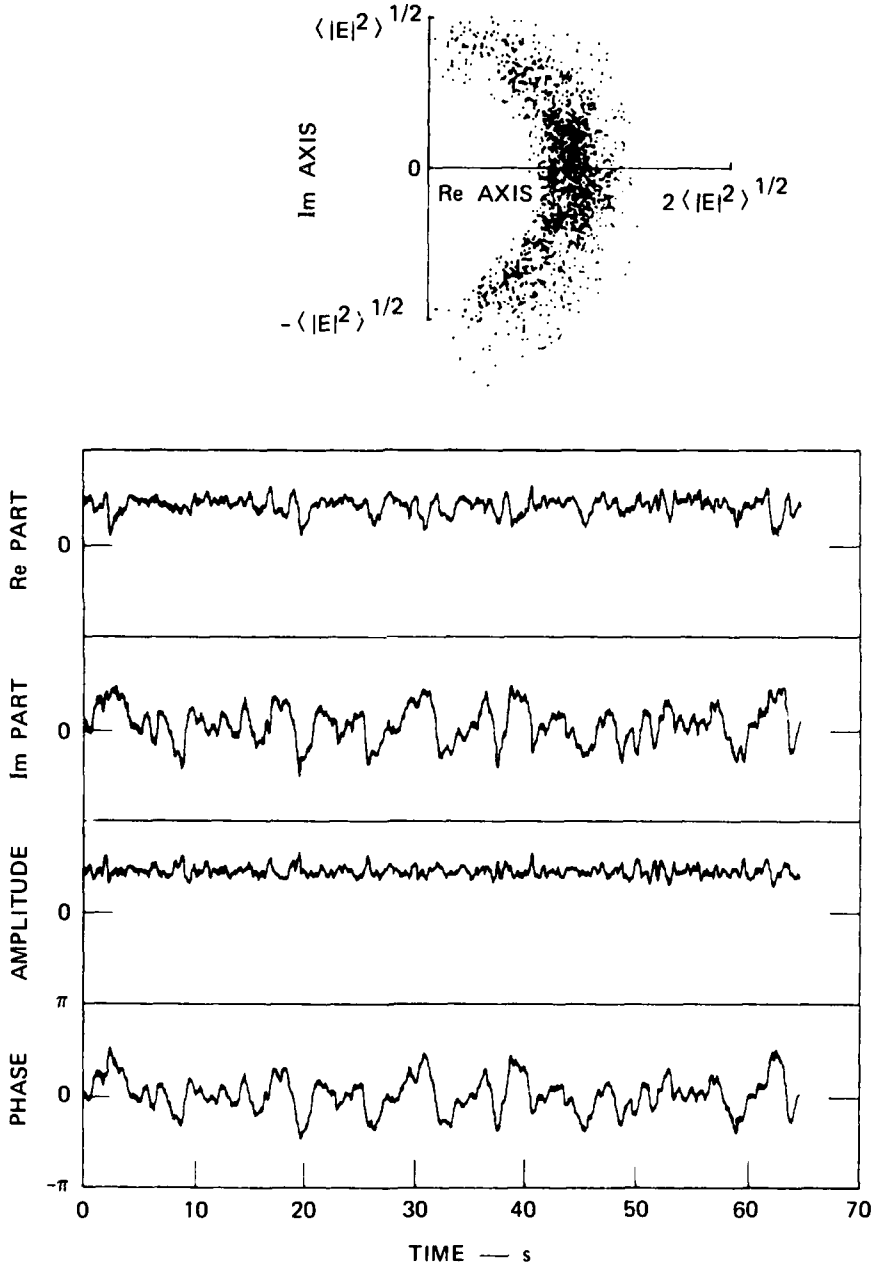

FIGURE 2 FIRST ORDER STATISTICS OF A SIGNAL UNDERGOING WEAK SCINTILLATION (S_4 = 0.29)

Figures 3 and 4 (see Fremouw et al., 1976a, for details of the separation procedure). From the scatter diagram shown in the top part of Figure 3 we see that $\sigma_h^2 < \eta^2$. Moreover, because of the rotated elliptical form of the scatter diagram $\sigma_x^2 < \sigma_y^2$ and the correlation coefficient, ρ_{xy}, is negative (Rino and Fremouw, 1973; Rino et al., 1976).

From the scatter diagram in the top part of Figure 4, we see similarly that $\sigma_\chi^2 \ll \sigma_\phi^2$. A careful inspection will show that the amplitude and phase are anticorrelated. From a ray-optics viewpoint, this is expected since phase depletions cause focusing and vice versa. Indeed, the same argument can be applied to reconcile the fact that $\rho_{xy} < 0$; since, for weak scatter ($\sigma_h^2 \ll 1$), the phase-quadrature component approximates the signal phase perturbation, and the in-phase component approximates the fractional amplitude perturbation.

An example of severe scintillation is shown in Figure 5. The scatter diagram for the composite signal [Figure 5(a)] appears to be Rayleigh. We see from Figures 5(b) and 5(c), however, that the scatter component retains a measurable coherent part, and the focus component is dominated by large slow phase variations.

Thus, while the overall fading structure of the channel for severe scintillation is reasonably well approximated by a Rayleigh distribution, the time structure of the signal amplitude and phase are very different. The analysis presented in the remainder of this section lays the foundations for calculating the impact of this model on representative communication systems.

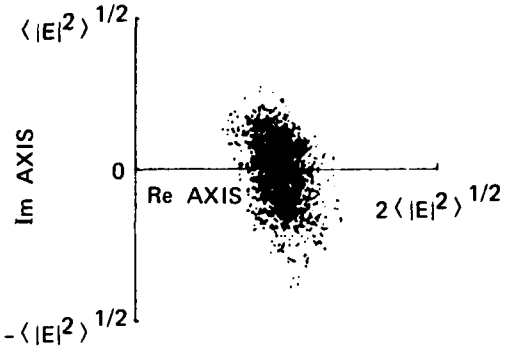

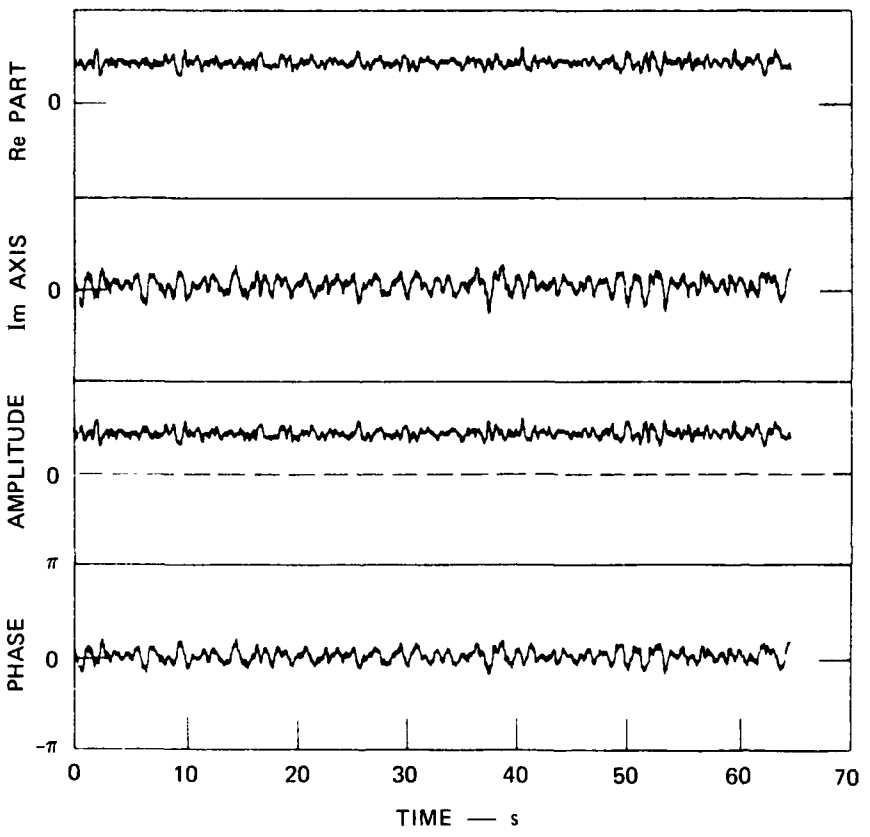

FIGURE 3 "SCATTER" COMPONENT OF THE SIGNAL IN FIGURE 2 (containing intensity and phase fluctuations in the spectral range greater than 0.4 Hz)

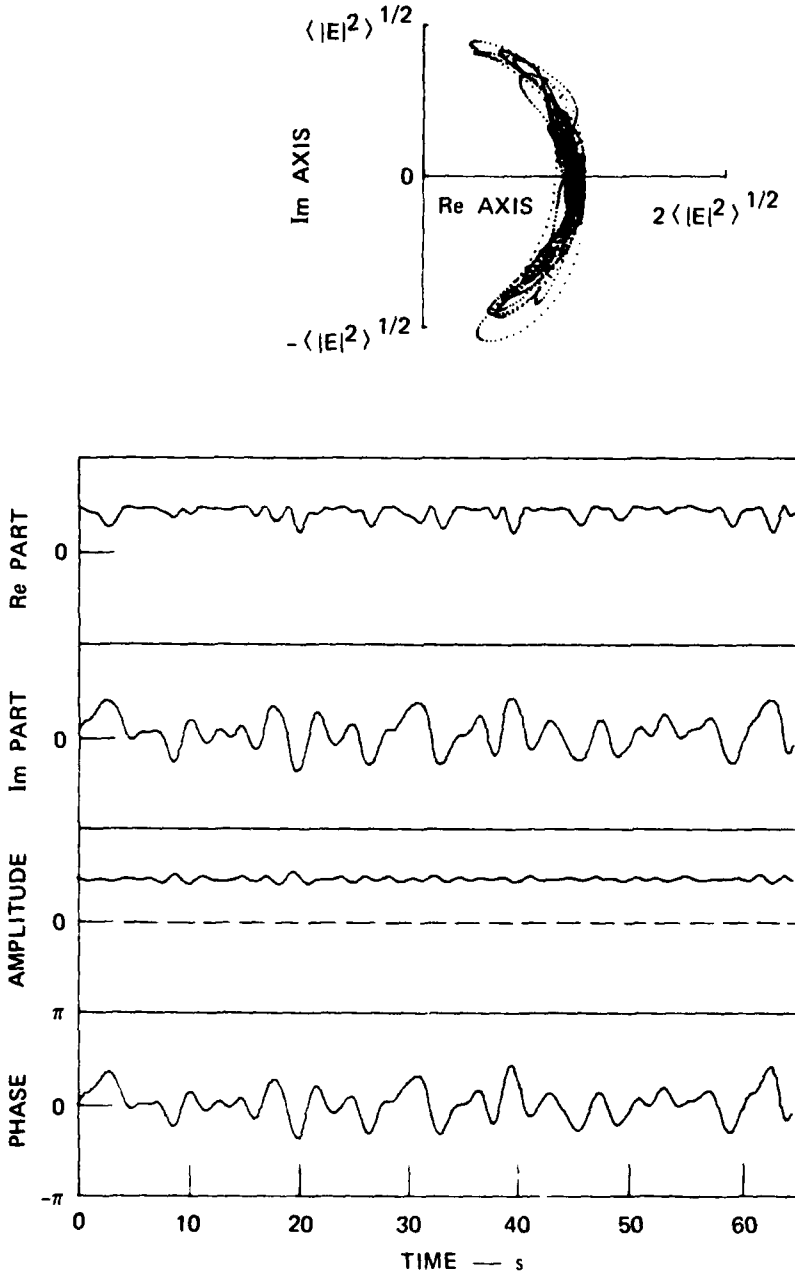

FIGURE 4 THE "FOCUS" COMPONENT OF THE SCINTILLATING SIGNAL IN FIGURE 2 CONSISTING OF PHASE AND LOG-AMPLITUDE VARIATIONS IN THE SPECTRAL RANGE FROM 0.1 TO 0.4 Hz

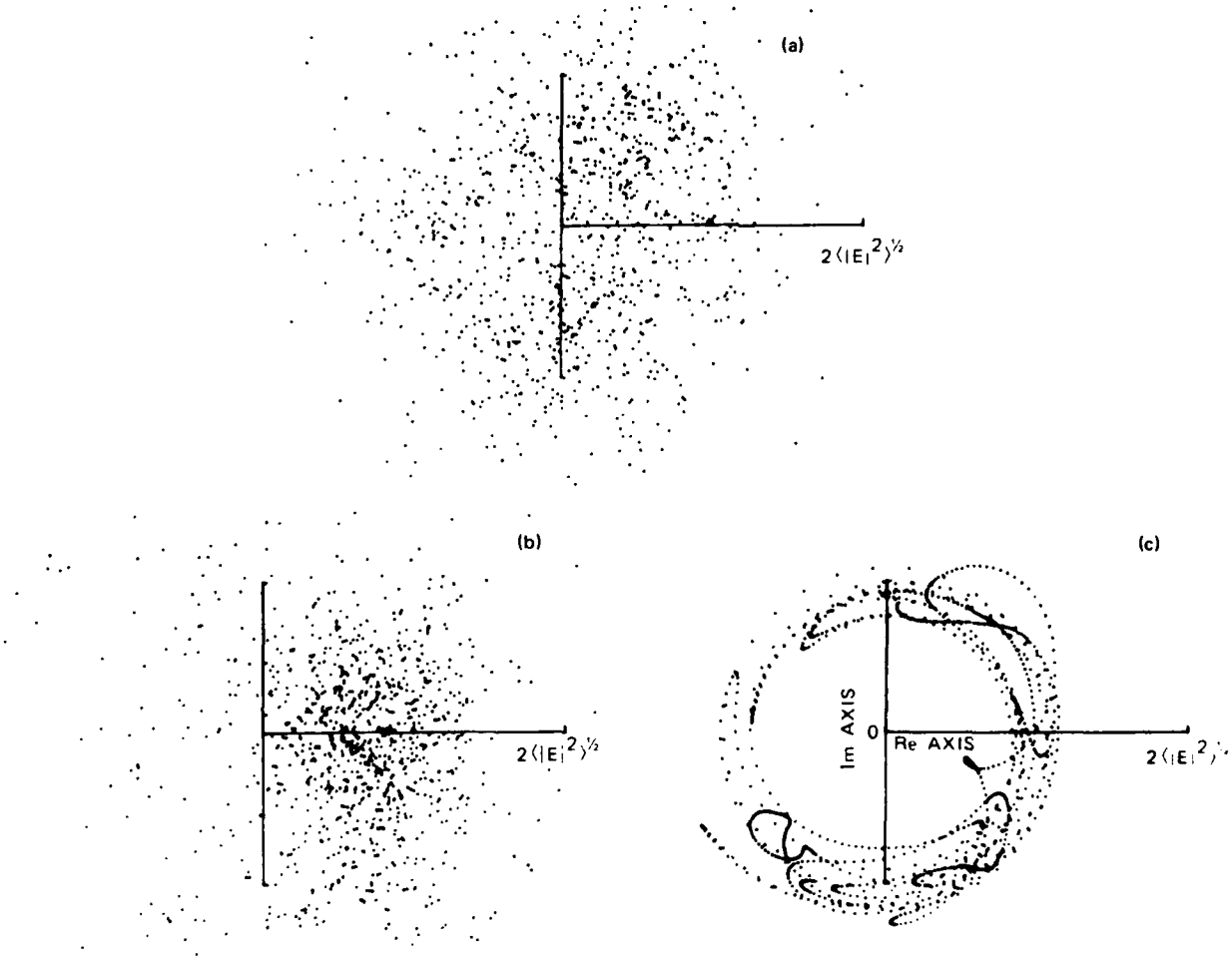

FIGURE 5 SCATTER PLOTS OF (a) COMPOSITE SCINTILLATING SIGNAL, (b) SCATTER COMPONENT, AND (c) FOCUS COMPONENT RECORDED UNDER STRONG SCINTILLATION (S_4 = 0.89) CONDITIONS. Transit over Poker Flat, Alaska, 2022:41 to 2023:21 GMT, 3 October 1975.

II ERROR-RATE DETERMINATION

Derivation

In this section, we shall obtain an expression for the probability of error over the two-component channel for the canonic receiver shown in Figure 6. This canonic receiver is a general structure that can be made mathematically equivalent to several types of binary diversity receivers (such as FSK, DPSK, fixed reference PSK) by the proper choice of the two input filters and the quadratic combiner (see Appendix A). The method is a generalization of the procedure developed by Bello and Nelin (1962a,b). We assume that the outputs of the diversity branches, d_i, are statistically independent and identically distributed. Complex signal notation is used throughout.

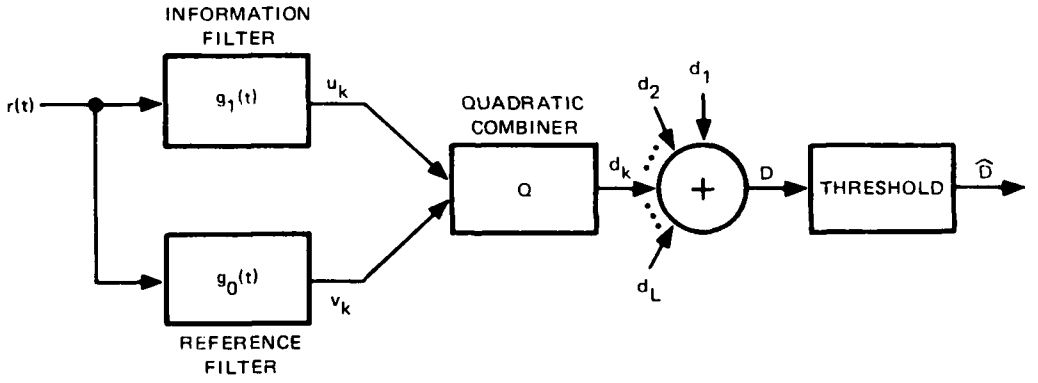

FIGURE 6 CANONIC BINARY RECEIVER STRUCTURE

The outputs u_k and v_k, of the information and reference filters in Figure 6 can be expressed as

$$u_k = \int r_k(t)\, g_1(t)\, dt \quad , \tag{10}$$

and

$$v_k = \int r_k(t)\, g_o(t)\, dt \quad , \tag{11}$$

where the limits of integration depend upon g_1 and g_o (see appendix).

If we make the definitions

$$\begin{aligned} u_k &= u_{k1} + j u_{k2} \quad , \qquad \text{(a)} \\ v_k &= v_{k1} + j v_{k2} \quad , \qquad \text{(b)} \end{aligned} \tag{12}$$

and define the column vector

$$\underline{x}_k = (u_{k1},\ u_{k2},\ v_{k1},\ v_{k2})^T \tag{13}$$

(the T denotes transpose), the output of the kth quadradic combiner, d_k, can be written as

$$d_k = \underline{x}_k^T\, Q\, \underline{x}_k \quad , \tag{14}$$

where Q has the form

$$Q = \begin{bmatrix} a & 0 & c_1 & c_2 \\ 0 & a & -c_2 & c_1 \\ c_1 & -c_2 & b & 0 \\ c_2 & c_1 & 0 & b \end{bmatrix} \quad . \tag{15}$$

The decision variable D then is

$$D = \sum_{k=1}^{L} \underline{x}_k^T Q \underline{x}_k \quad , \tag{16}$$

in which the L terms are mutually independent.

Defining terms appropriately, the error probability takes the form

$$P_e = \text{Prob}\left\{D < 0 \,|\, s_1(t) \text{ transmitted}\right\} \quad . \tag{17}$$

To make the problem tractable, we take advantage of the slow variation of the focus component and assume that $\exp \psi(t)$ is constant over the sample interval $0 \le t \le T$. With this assumption, the joint distribution of the random vector $\underline{x}_k$ is Gaussian, conditioned on the value of the log-normal part. We then determine that

$$P_{e|\psi} = \text{Prob}\left\{D < 0 \mid s_1(t),\ e^{\psi_k(t)} = \alpha_k\right\} \quad , \tag{18}$$

and average over α to evaluate the unconditioned probability P_e.

To determine the probability distribution of D, we first compute the characteristic function for $d_k = \underline{x}_k^T Q \underline{x}_k$. This is a quadratic form in a Gaussian random vector; the characteristic function is known and given by

$$C_d(\zeta) = \overline{e^{j\zeta d_k}} = \frac{\exp\left\{-1/2\ \overline{\underline{x}_k^T}\, R_k^{-1}\left[I - (I - 2j\zeta R_k Q)^{-1}\right]\overline{\underline{x}_k}\right\}}{\det\left\{I - 2j\zeta R_k Q\right\}} \quad , \tag{19}$$

where R_k is the covariance matrix

$$R_k = \overline{(\underline{x}_k - \bar{\underline{x}}_k)(\underline{x}_k - \bar{\underline{x}}_k)^T} \quad . \tag{20}$$

Equation (19) can be written in a form more suitable for computation in terms of the eigenvalues and eigenvectors of the matrix RQ. Using simple matrix manipulations,

$$C_d(\zeta) = \frac{e^{-\underline{x}^T \, QM\Gamma \, M^{-1}\underline{x}}}{\prod_{i=1}^{4} (1 - 2j\zeta\lambda_i)^{1/2}} \tag{21}$$

where the λ_i are the eigenvalues of RQ, and M is the matrix of eigenvectors of RQ (sometimes called the modal matrix). That is:

$$RQ = M \, \Lambda \, M^{-1} \quad , \tag{22}$$

where

$$\Lambda = \text{diag}\{\lambda_i\} \quad ; \tag{23}$$

also,

$$\Gamma = \text{diag}\left\{\frac{j\zeta}{1 - 2j\zeta\lambda_i}\right\} \quad . \tag{24}$$

The relationship between the characteristic function and the error probability is given by Parzen (1960):

$$P_{e|\psi} = 1/2 - \frac{1}{\pi}\int_0^\infty \frac{\text{Im}\{C_D(\zeta)\}}{\zeta} \, d\zeta \quad , \tag{25}$$

where $C_D(\zeta)$ is the characteristic function of the decision variable D. Using the fact that the diversity outputs are independent and identically distributed, we have

$$P_{e|\psi} = 1/2 - \frac{1}{\pi}\int_0^\infty \frac{\text{Im}\{[C_d(\zeta)]^L\}}{\zeta} \, d\zeta \quad . \tag{26}$$

Averaging over ψ (and interchanging orders of integration and averaging) we obtain

$$P_e = 1/2 - \frac{1}{\pi} \int_0^\infty \frac{\overline{\mathrm{Im}\left\{[C_d(\zeta)]^L\right\}}}{\zeta} \, d\zeta \quad . \tag{27}$$

III NUMERICAL EVALUATION OF P_e

A. Introduction

Equation (27) is the complete general expression for the error rate using the two-component channel model. Like many general expressions, its evaluation is difficult and costly. The reason in this case is that Equation (27) requires performing a three-dimensional numerical integration to a very high degree of accuracy, as P_e is given by the difference between one-half and the result of the integration. Although we have performed this integration for several examples, we also have considered several, more easily evaluated, special cases that provide insight into the relationship between P_e and the channel scintillation parameters. These special cases are obtained by turning off one of the two portions of the model. The resulting two single-component-channel models--the scatter (only) channel shown in Figure 7 and the focus (only channel shown in Figure 8--are important in their own right. The scatter channel can characterize Rayleigh or Rician fading channels as well as more general situations where $\sigma_x \neq \sigma_y$ and $\rho_{xy} \neq 0$. The focus (only) channel is the model for log-normal fading.

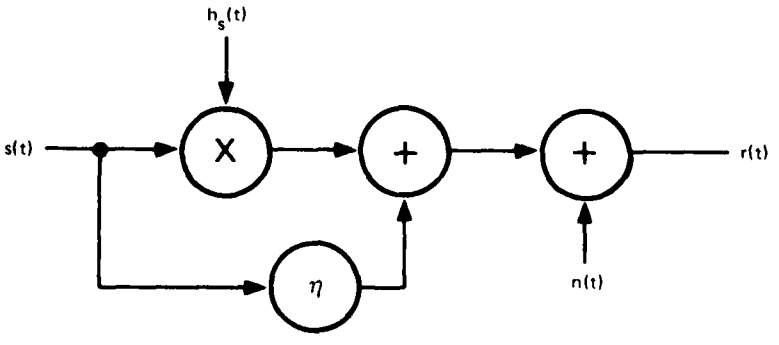

FIGURE 7 SCATTER (only) CHANNEL MODEL

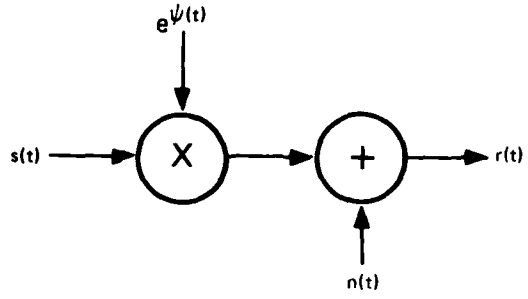

FIGURE 8 FOCUS (only) CHANNEL MODEL

In the following sections, we present results of our numerical evaluations of P_e for both single-component channels and the two-component channel for FSK and DPSK communication systems. Some of the details of the receiver setup (i.e., the way in which the receiver was specialized for the two types of modulations) and the computation procedures are given in Appendix A. For all computations, the noise was assumed to be stationary white Gaussian.

B. Single-Component Channels

1. The Scatter Component

For the scatter channel, the received signal is given by

$$r(t) = [\eta + h_s(t)]\, s(t) + n(t) \quad . \tag{28}$$

This model is perhaps the most useful of the two because it reduces to the Rician channel when $\sigma_x^2 = \sigma_y^2$ and to the Rayleigh channel with the added constraint $\eta = 0$. Furthermore, $\eta = 1$ corresponds to the non-fading, additive noise channel.

To characterize the received signal r(t) we must know the following parameters--in addition to the input waveform s(t):

- η^2 (the energy in the coherent portion--note that this fixes the energy in the scatter portion--see Eq. 4).
- The SNR.
- $\frac{\sigma_x^2}{\sigma_y^2}$ (the ratio of the in-phase power to the quadrature power).

- ρ_{xy} (the correlation coefficient between the in-phase and quadrature terms.
- τ/T [the correlation time of the scintillation (τ) relative to the bit duration (T); τ^{-1} is the half-power bandwidth for a gaussian fading spectrum (see Appendix)].

a. Coherent Component Variations

The lossless channel [Eqs. (7), (8)] has, in effect, normalized the channel so the coherent component η is restricted to the range 0 to 1. Figure 9 shows how the power in the coherent component, η^2, affects P_e at an SNR of 20 dB for slow and fast fading. Observe that, for slow fading, the error rate for DPSK is always lower than the FSK error rate. For fast fading, however, the FSK error rate is lower for $\eta^2 \lesssim 0.6$. The reason for this behavior is that FSK is inherently better than DPSK in fast-fading regimes (Bello and Nelin, 1962b), but DPSK is better when the fading is slow or non-existent. As the magnitude of the coherent component increases, the effects of fading become less and less significant, and DPSK becomes the lower error-rate system. Note also that P_e does not begin to show a significant reduction until over one-half the power is in the coherent component ($\eta^2 > 0.5$). This is of significance for obtaining approximate error rates for situations in which some coherent component is present, but the fading dominates.

b. σ_x^2/σ_y^2 Variations

The division of the scintillating portion of the received signal into in-phase and quadrature components is given by the ratio σ_x^2/σ_y^2. If the scatter ellipse (see Figure 3) is oriented vertically, i.e. $\rho_{xy} = 0$, then this ratio is also equal to the axial ratio of the ellipse. For weak scintillation, the in-phase component corresponds (in an approximate sense) to amplitude scintillation, and the quadrature component corresponds to phase scintillation. Figure 10 shows the relationship between P_e and σ_x^2/σ_y^2 for slow and fast scintillation for $\eta^2 = 0.75$, $\rho_{xy} = 0$ and

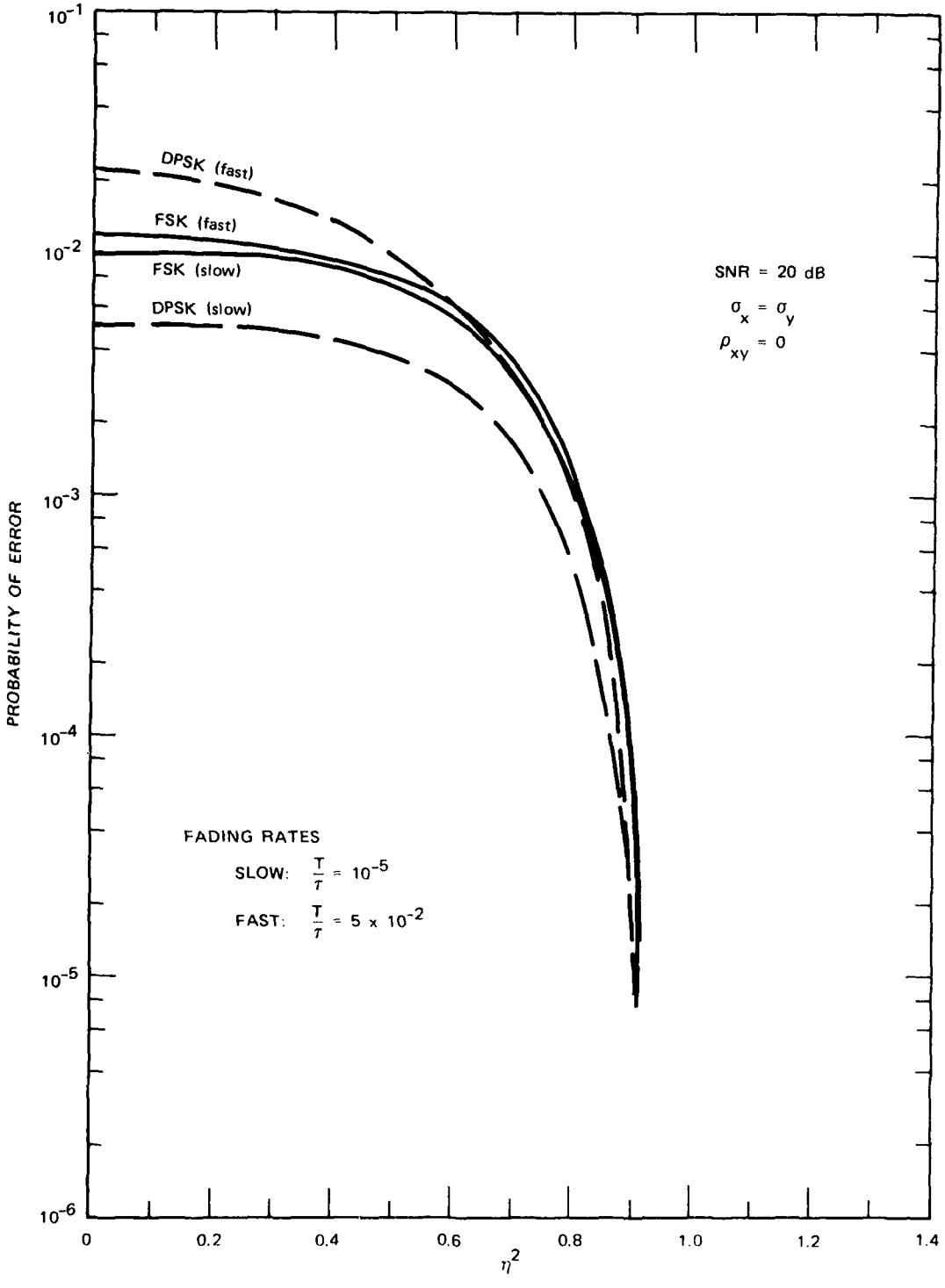

FIGURE 9 EFFECT OF THE NORMALIZED COHERENT COMPONENT IN RICIAN CONDITIONS

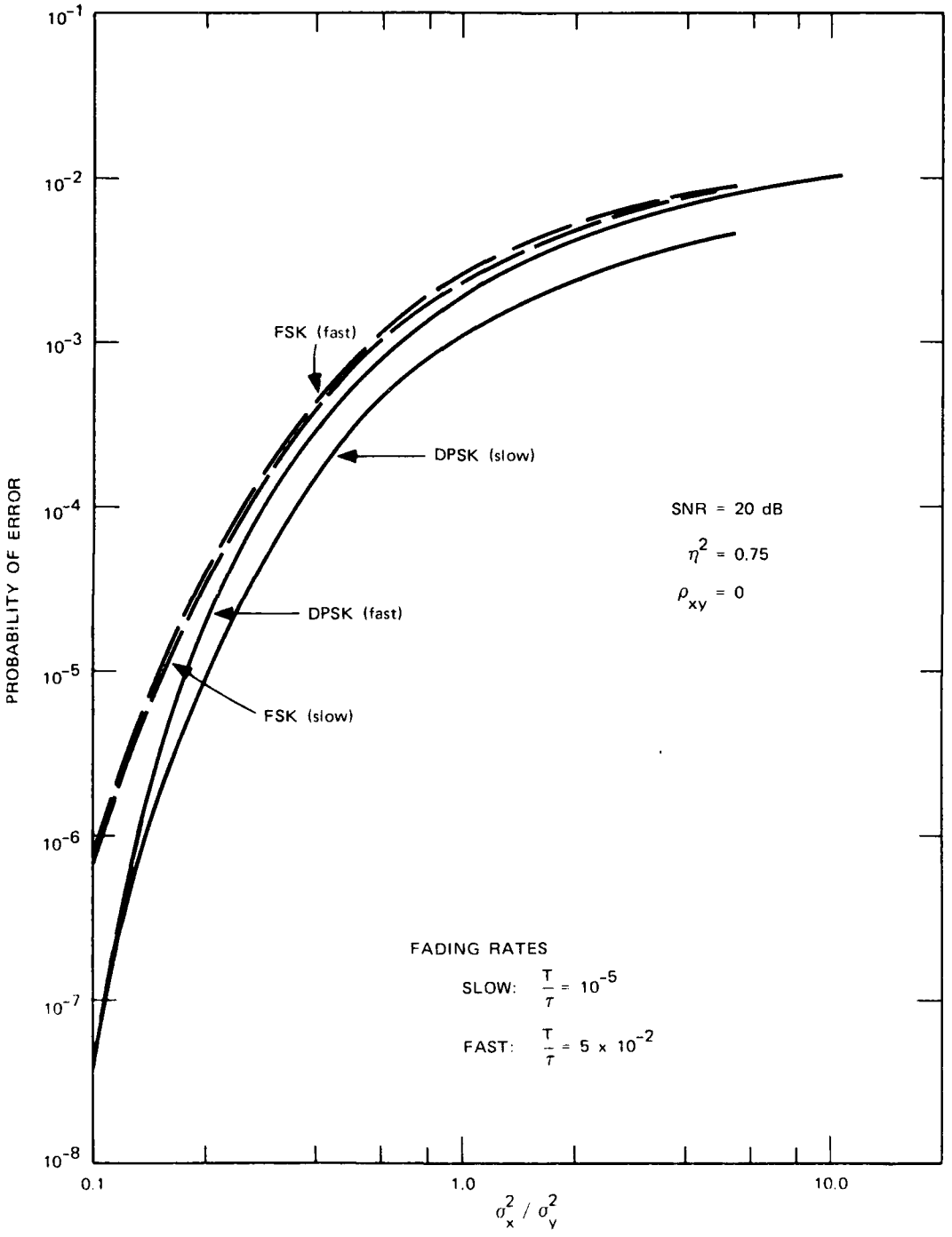

FIGURE 10 ERROR RATE vs. σ_x^2 / σ_y^2

a 20 dB SNR. The error rate drops rapidly as signal power is transferred from the in-phase to the quadrature component for both forms of modulation and both scintillation rates. This figure gives an indication of the harmful effect of amplitude fading relative to phase scintillations--at least for FSK and DPSK. Coherent phase systems (coherent PSK), which are known to be more sensitive to rapid fading, would probably not show such a dramatic reduction in P_e as σ_x^2/σ_y^2 decreases. Figure 11 shows P_e as a function of the SNR with σ_x^2/σ_y^2 as a parameter.

c. Correlation Coefficient Variations

The correlation coefficient ρ_{xy} has significant effect on the error rate as shown in Figures 12 and 13. (The severe drop in P_e occurs for larger values of ρ_{xy} (> 0.5) and is probably not a situation likely to occur in real life.) The rapid fall of P_e as $\rho_{xy} \rightarrow 1$ is because the random scintillation is becoming more ordered and, in the process, developing a lower limit on the possible amplitude excursions. For example, the line L in Figure 14 is the limit of the scatter plot as $\rho \rightarrow -1$ when $\eta^2 = 0.75$ and $\sigma_x^2/\sigma_y^2 = 0.5$. The signal amplitude can never drop below the distance of closest approach of L to the origin (the line OA); hence the amplitude fading has developed a lower limit. This lower limit is important because the main reason fading increases the error rates as much as it does is the finite probability that a deep fade will occur and the signal will drop into the noise.

d. Fading Rate

The influence of fading rate on P_e has been examined for Rayleigh fading by Bello and Nelin (1962b); however, we have been unable to find a study of the fading rate in connection with any other type of fading (such as Rician). Bello and Nelin show that the fading rate establishes a lower limit to the error rate, termed the irreducible probability of error (P_{IR}). Once this limit is reached, further increases in the SNR will not result in reductions in P_e.

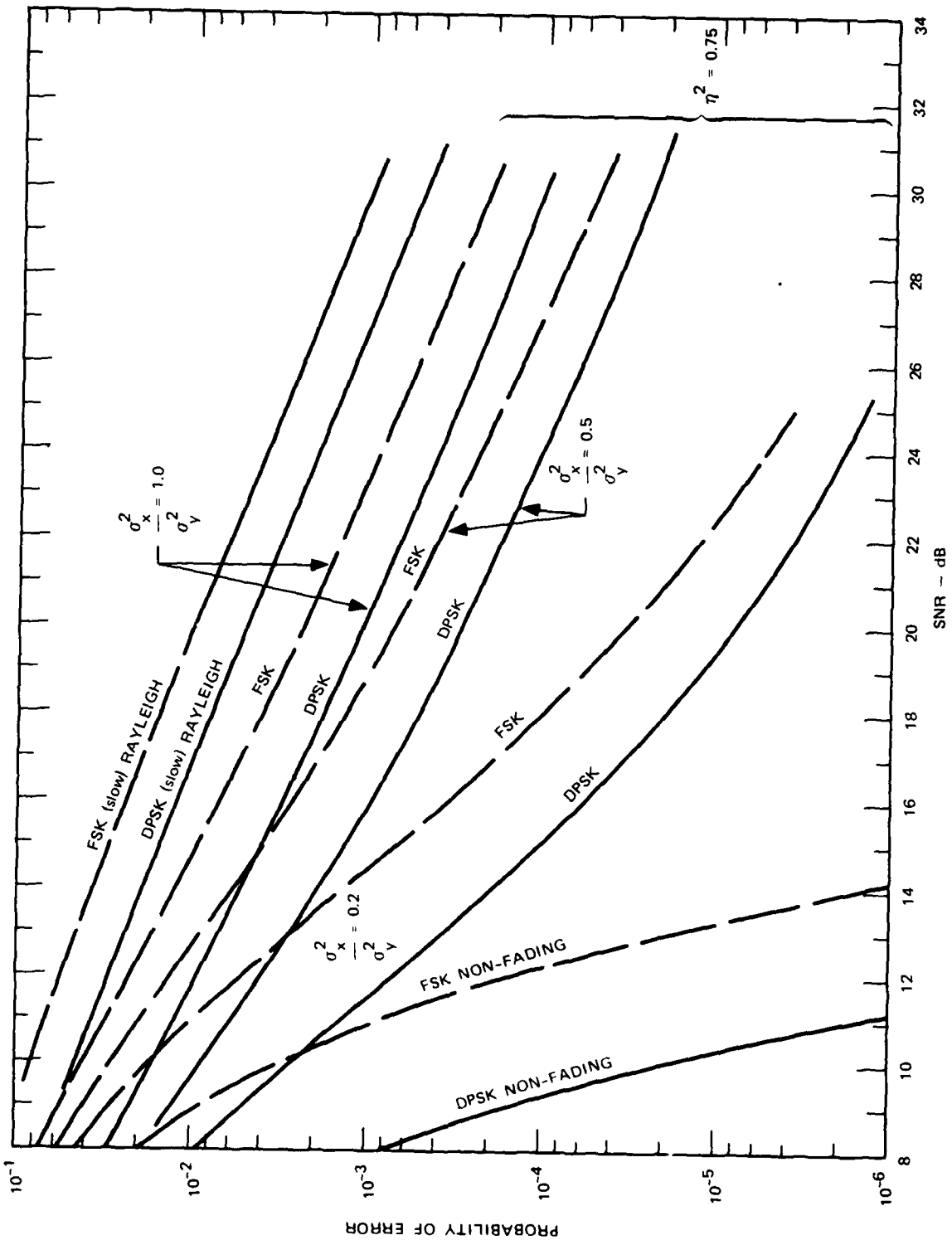

FIGURE 11 ERROR RATE vs. SNR FOR DIFFERENT VALUES OF σ_x^2 / σ_y^2

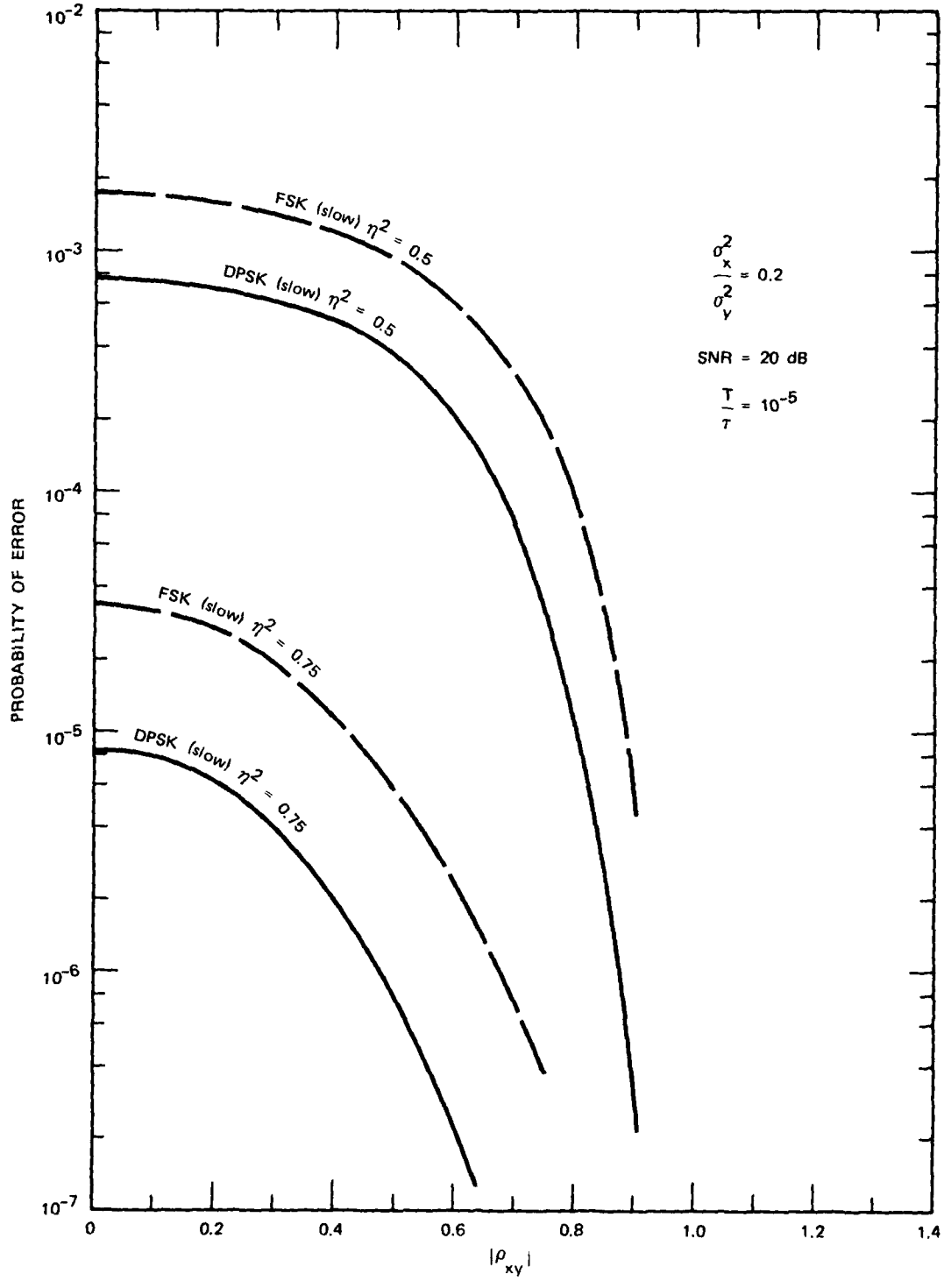

FIGURE 12 EFFECT OF CORRELATION BETWEEN x AND y SCATTER COMPONENTS

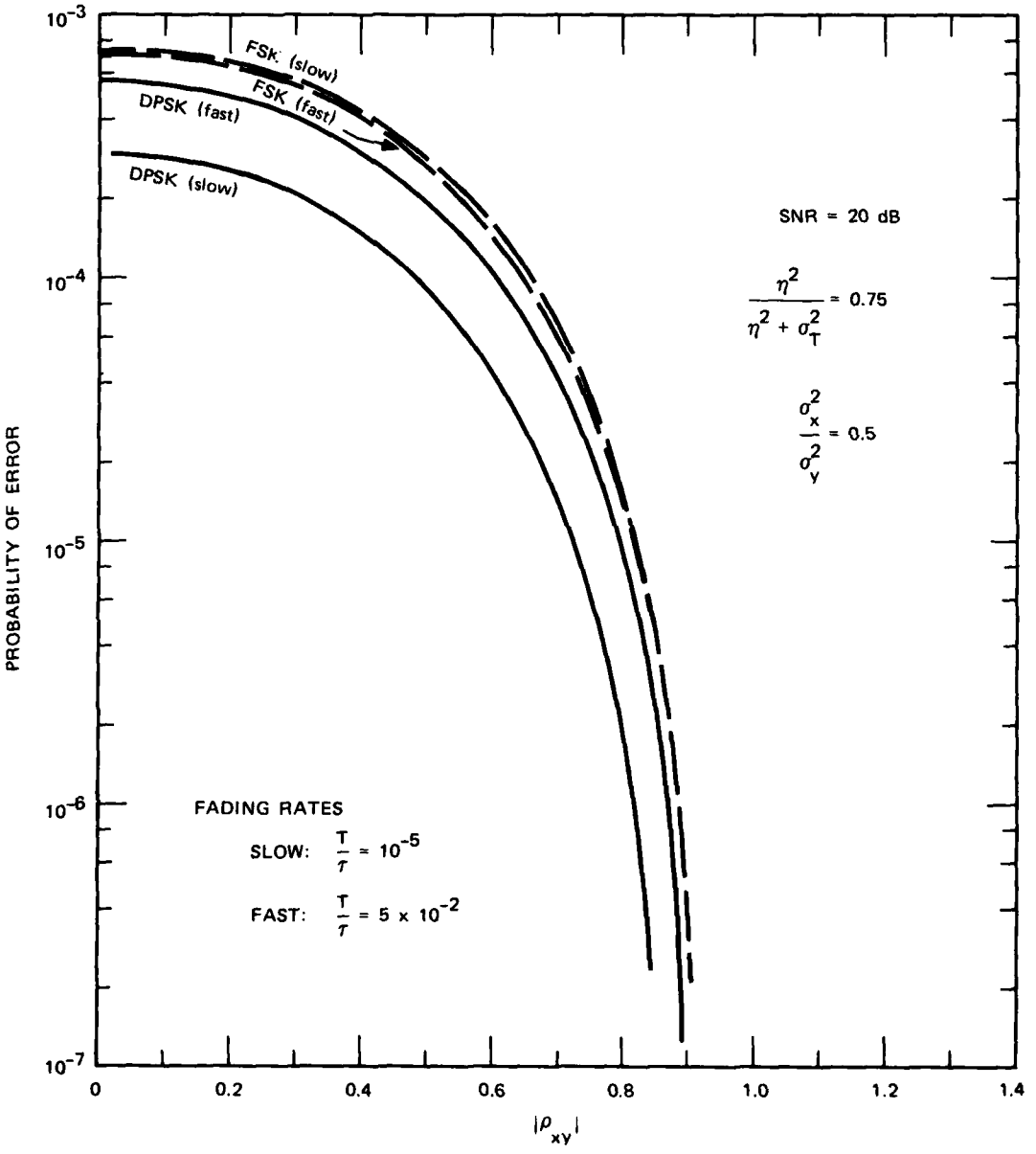

FIGURE 13 EFFECT OF CORRELATION BETWEEN x AND y SCATTER COMPONENTS

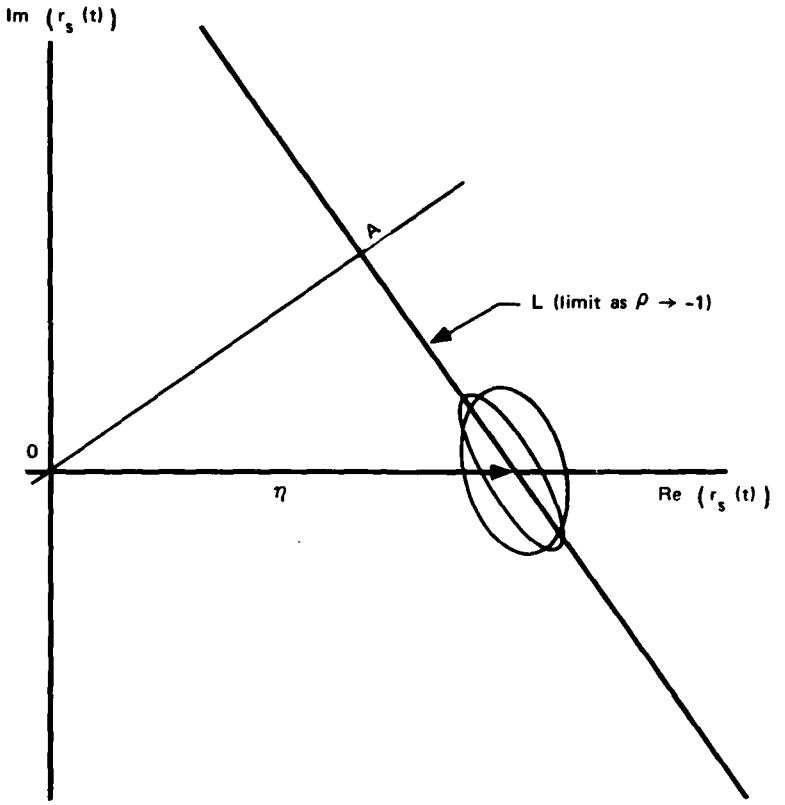

FIGURE 14 SCHEMATIC DRAWING OF SCATTER DIAGRAM ELLIPSE AS $\rho_{xy} \rightarrow -1$

An irreducible probability of error is also established by the scintillation rate of our 'scatter' channel, given fixed values of η^2, ρ_{xy} and σ_x^2/σ_y^2. Figure 15 shows the P_{IR} versus the relative fading bandwidth (T/τ) for Rician conditions ($\sigma_x^2/\sigma_y^2 = 1$, $\rho_{xy} = 0$) for several values of η^2 including $\eta^2 = 0$ (Rayleigh fading). It is interesting that the Rician curves show the same slope as the Rayleigh curves, differing only by a fixed offset due to the coherent component.

Figure 16 shows P_{IR} for non-Rician conditions. The behavior is much the same as the Rician channel shown in Figure 15 except for $\sigma_x^2/\sigma_y^2 = 0.2$. Here, the difference between DPSK and FSK increases dramatically as the fading bandwidth increases with the DPSK system obviously affected by the rapid phase changes due to the scintillation.

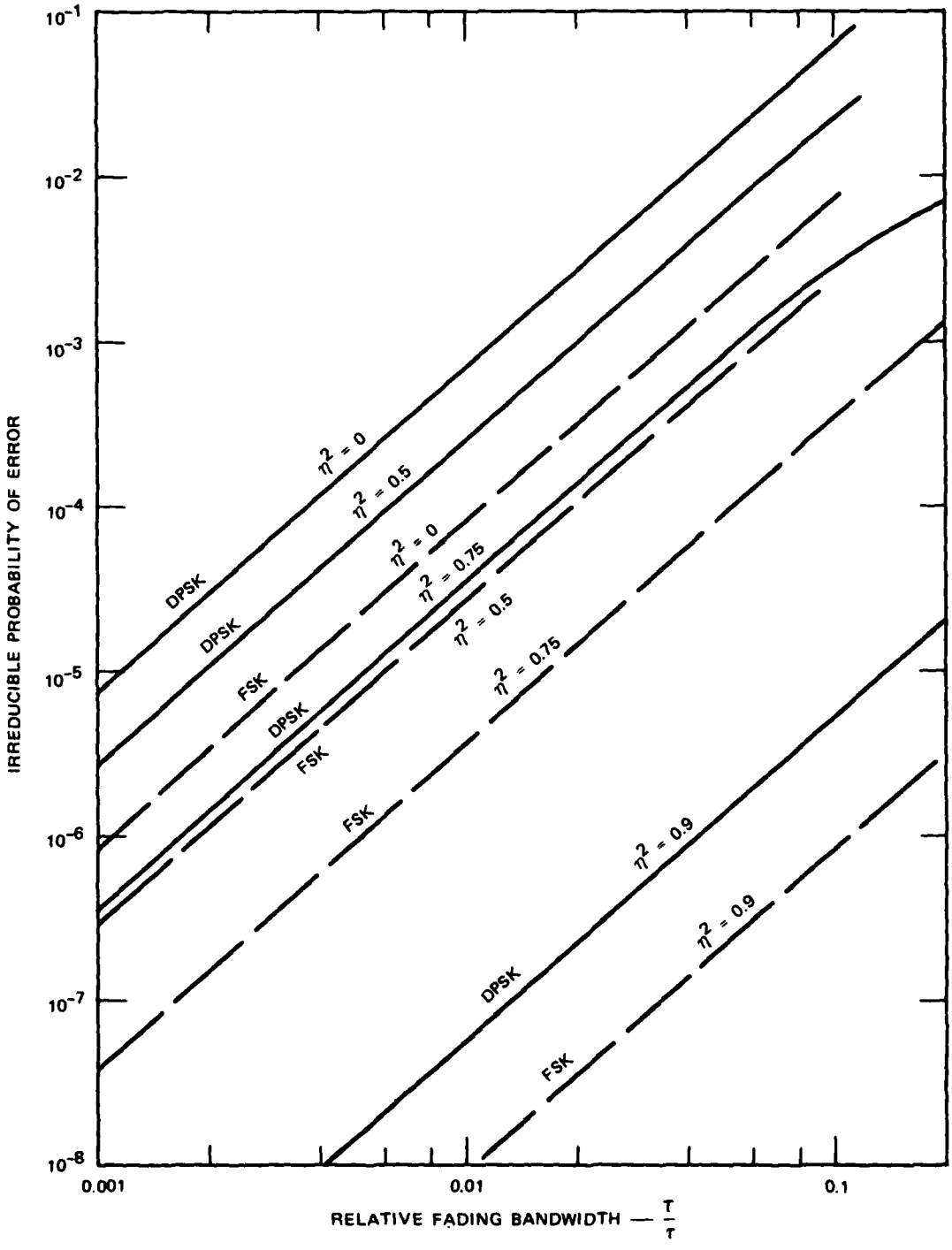

FIGURE 15 IRREDUCIBLE PROBABILITY OF ERROR FOR RICIAN CHANNELS

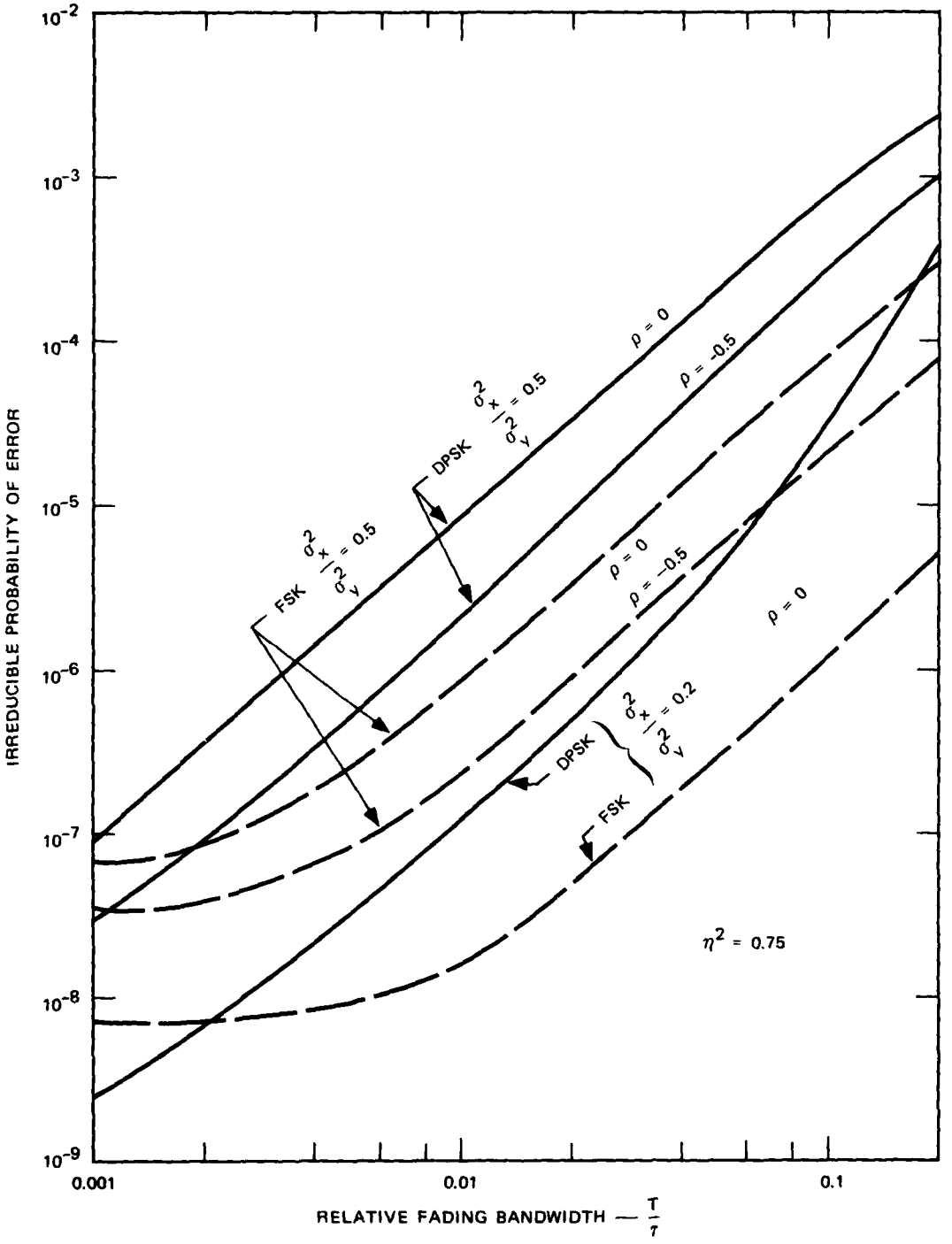

FIGURE 16 IRREDUCIBLE PROBABILITY OF ERROR FOR NON-RICIAN CHANNELS

The flattening-out at the low end of the curves is probably because this range of P_e is beyond the limit of accuracy of the integration.

2. The Focus Component

The other half of the two-component model, the focus channel, is essentially a slow-fading log-normal channel. We have only performed computations for slow log-normal amplitude fading (i.e., $\sigma_\chi \neq 0$, $\sigma_\phi = 0$, $\rho_{\chi\phi} = 0$), shown in Figure 17. These are identical with results obtained by numerical integration of the standard expression for the probability of error in a slow-fading channel

$$P_e = \int_{-\infty}^{\infty} f(x)\ P(x)dx \quad , \tag{29}$$

where x is the SNR, P(x) is the log-normal probability distribution, f(x) is the probability of error for DPSK or FSK in a non-fading channel, i.e.,

$$f(x) = \begin{cases} 1/2e^{\frac{-x}{2}} & \text{FSK} \\ 1/2e^{-x} & \text{DPSK} \end{cases} . \tag{30}$$

C. Two-Component Channels

The error rate for the two-component channel was determined for the examples of moderate and severe scintillation used by Scott and Knepp (1978) of MRC. The channel parameters and resulting error rates are given in Table 1. The error rates we obtain for moderate scintillation are much higher than those obtained by MRC and cannot be explained by the difference in modulation schemes. Indeed, DPSK or FSK should perform better than PSK in the rapid scintillation of this channel. A possible cause of this discrepancy is the small sample size used by Scott and Knepp (they used a Monte Carlo simulation with a sample size of $\sim$ 3000 to estimate P_e. Our approach does not have this limitation.

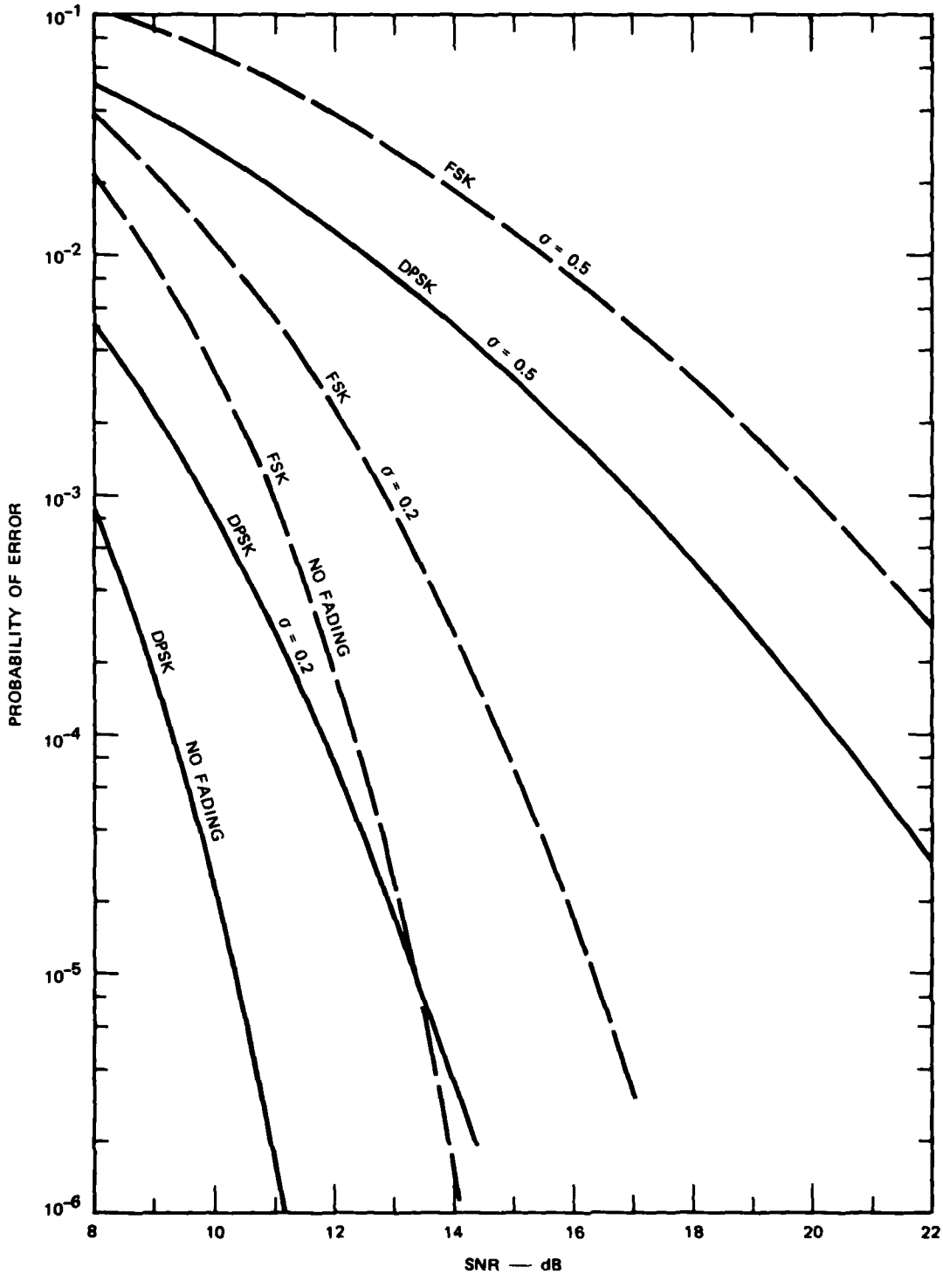

FIGURE 17 PROBABILITY OF ERROR FOR SLOW LOG-NORMAL FADING

Table 1

SUMMARY OF CHANNEL PARAMETERS

Channel Parameter	Moderate Scintillation		Severe Scintillation	
	MRC*	SRI†	MRC*	SRI†
Scatter Component				
S_4 index	0.5920		0.9825	
η^2		0.411		0.0174
σ_x	0.2922		0.9164	
σ_y	0.4585		0.8756	
σ_x^2/σ_y^2	0.4061	0.4061	1.0952	1.0952
ρ_{xy}	-0.2039	-0.2039	-0.0022	-0.0022
τ/T‡		0.041		0.111
Focus Component				
S_4 index	0.2569		0.4416	
σ_χ	0.1282	0.1282	0.209	0.209
σ_ϕ	1.3328	1.3328	3.6563	3.6563
$\rho_{\chi\phi}$	-0.5435	-0.5435	-0.1376	-0.1376
τ/T‡	0.0013	0		0
Error Probabilities				
P_e (PSK)§	0.39×10^{-3}		0.23×10^{-1}	
P_e (DPSK)§		0.197×10^{-1}		0.865×10^{-1}
P_e (FSK)§		0.151×10^{-1}		0.345×10^{-1}

*MRC = Values given by Scott and Knepp (1978).

†SRI = Normalized MRC values suitable for our computations.

‡Scott and Knepp used a data rate of 75 bits/sec.

§A mean SNR of 16.25 dB was used.

In addition to the computations shown in Table 1, we varied the focus parameters (σ_χ, σ_ϕ and $\rho_{\chi\phi}$) above and below the moderate scintillation levels and computed the resulting error rates. Neither σ_ϕ nor $\rho_{\chi\phi}$ had any effect whatsoever on P_e. This is understandable when one recalls that DPSK is a differential system and should be transparent to slow phase variations. Of course, FSK will also be transparent to slow phase variations. On the other hand, a system employing fixed-reference PSK will be severely degraded by any phase variations--fast or slow.

The error rate was affected by variations of σ_χ, as shown in Figure 18. However, P_e is not a sensitive function of this parameter at the level of the other scintillating parameters of this example. (The principal determinants of P_e in this example are the SNR and the fading rate.)

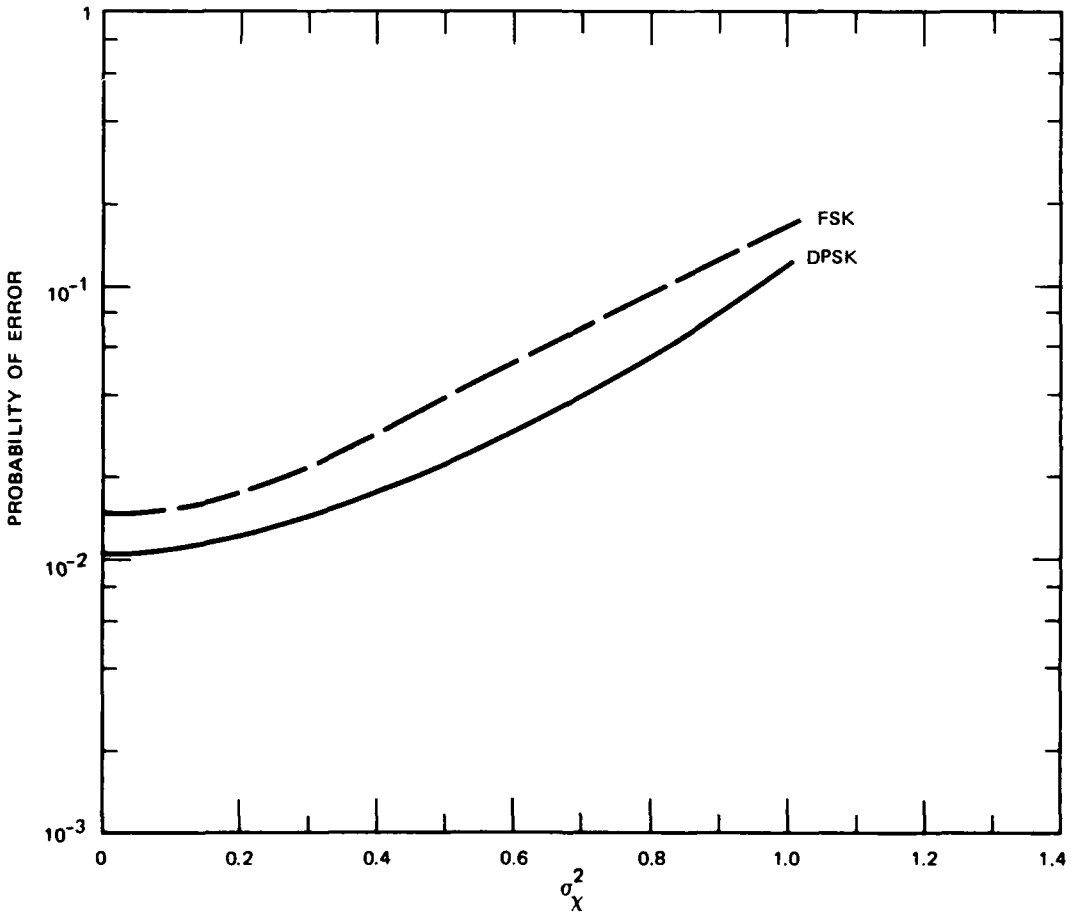

FIGURE 18 EFFECT OF VARYING σ_χ UNDER MODERATE SCINTILLATION CONDITIONS

IV CONCLUSIONS

The two-component channel model provides both a means of calculating the probability of error for the transionospheric channel and an insight to the mechanism of error generation. Although extensive evaluation of the complete expression for P_e (to study a system under many different conditions, for example) would be costly, it is feasible. Also, the model lends itself to simplifications that allow special cases to be studied economically and easily.

Real channels do not have an unlimited range of possible parameter variations. Furthermore, the statistics of these parameters (means, variances, etc.) are usually not independent of one another even if the parameter values themselves are independent. For example, a high scatter scintillation index (low η^2) will usually mean a high value of σ_χ^2 as well. Hence, studying a system under conditions that are likely to occur in operation does not necessarily mean performing an inordinately large number of computations.

The dominant source of errors induced by transmitting through the two-component channel is the scatter component. The scatter component controls the amount of coherent signal and the amplitude and rapidity of the fast scintillations. These parameters, together with the noise, are the most critical aspects of the signal. The focus component has only a secondary effect on P_e, at least when it is present in the same relative proportions as seen in our examples. For the modulation schemes we have examined, the focus term can almost be viewed as a simple log-normal perturbation on the scatter component.

Although Eq. (27) is expressed in terms of an L-branch diversity receiver, all of our analysis has been for L = 1, i.e., no diversity. This is because considerable study has already been directed toward the effects of diversity reception and the general behavior of diversity systems is reasonably well understood. Our principal intention has been to study the way in which various channel parameters affect the error rate.

REFERENCES

Bello, P., and Nelin, B. D., "Predetection Diversity Combining with Selectively Fading Channels," IRE Trans on Comm Systems, Vol. CS-10, p. 32 (March 1962a).

Bello, P., and B. D. Nelin, "The Influence of Fading Spectrum on the Binary Error Probabilities of Incoherent and Differentially Coherent Matched Filter Receivers," IRE Trans on Comm Systems, Vol. CS-16, pp. 160-168 (June 1962b).

Fremouw, E. J., and C. L. Rino, Continued Modeling of Transionospheric Radio Propagation, Quarterly Technical Report 4, DARPA Contract No. F30602-75-C-0236, Stanford Research Institute, Menlo Park, CA (SRI Project 4259) August 1976b.

Fremouw, E. J., C. L. Rino, and R. C. Livingston, "A Two-Component Model for Scintillation," paper presented at Cospar Symposium, Boston, Massachusetts (1-4 June 1976a).

Fremouw, E. J., R. L. Leadabrand, R. C. Livingston, M. D. Cousins, C. L. Rino, B. C. Fair, and R. A. Long, "Early Results from the DNA Wideband Experiment--Complex Signal Scintillation," Radio Science, Vol. 13, No. 1 (January-February 1978).

Parzen, E., Modern Probability Theory and Its Applications, p. 402 (John Wiley & Sons, New York, 1960).

Rino, C. L., and E. J. Fremouw, "Statistics for Ionospherically Diffracted VHF/UHF Signals," Rad. Sci., 8, 223-233 (1973).

Rino, C. L., R. C. Livingston, and H. E. Whitney, "Some New Results on the Statistics of Radio Wave Scintillation: 1. Empirical Evidence for Gaussian Statistics," J. Geophys. Res., 81(13), 2051-2057 (1976).

Scott, R. C., and D. L. Knepp, "Comparison of Signal Scintillation Models," Topical Report for February 1978-June 1978, Report Number DNA 4652T, Contract No. DNA 001-77-C-0096, Mission Research Corp., Santa Barbara, CA (1978).

Appendix

DETAILS OF THE ERROR-RATE CALCULATION

FSK Receiver

For FSK, the information and reference filters in Figure 2 are matched to the mark and space waveforms; hence, the impulse responses are

$$\left.\begin{aligned} g_1(t) &= s_1^*(t) = \sqrt{2E/T}\, e^{\frac{-jn\pi t}{T}} \\ g_0(t) &= s_0^*(t) = \sqrt{2E/T}\, e^{\frac{+jn\pi t}{T}} \end{aligned}\right\} \quad 0<t<T \qquad \text{(A-1)}$$

where E is the total energy in the pulse, T is the pulse duration, and n is an integer equal to the frequency separation between the mark and space frequencies normalized with respect to 1/T (the asterisk denotes the complex conjugate). The quadratic combiner matrix is

$$Q = \begin{bmatrix} 1 & 0 & 0 & 0 \\ 0 & 1 & 0 & 0 \\ 0 & 0 & -1 & 0 \\ 0 & 0 & 0 & -1 \end{bmatrix} . \qquad \text{(A-2)}$$

DPSK Receiver

For DPSK the impulse responses of the receiver filters are

$$g_1(t) = s_1^*(t) - s_0^*(t) = 2\sqrt{2E/T} \qquad 0<t<T \qquad \text{(A-3)}$$

$$g_o(t) = g_1(t + T) \qquad -T<t<0 \quad , \qquad \text{(A-4)}$$

and

$$\left.\begin{aligned} s_1(t) &= \sqrt{2E/T} \\ s_0(t) &= -\sqrt{2E/T} \end{aligned}\right\} \quad 0<t<T \qquad \text{(A-5)}$$

The quadradic combiner matrix is

$$Q = \begin{bmatrix} 0 & 0 & 1 & 0 \\ 0 & 0 & 0 & 1 \\ 1 & 0 & 0 & 0 \\ 0 & 1 & 0 & 0 \end{bmatrix} \quad . \qquad \text{(A-6)}$$

Hence,

$$u_k = \int_o^T g_1(t) r_k(t) dt \quad , \qquad \text{(A-7)}$$

and

$$v_k = \int_{-T}^{o} g_1(t + T) r_k(t) dt = \int_o^T g_1(t) r_k(t - T) dt \quad . \qquad \text{(A-8)}$$

Note that the reference filter is identical to the information filter with the input delayed one bit duration.

R Matrix Computation

It is necessary to compute the covariance matrix

$$R = \overline{(\underline{x} - \bar{\underline{x}})(\underline{x} - \bar{\underline{x}})^T} \quad . \qquad \text{(A-9)}$$

This matrix is composed of auto- and cross-correlations of the real and imaginary parts of u and v (see Eqs. 9 and 10) such as

$$r_{11} = \overline{(u_1 - \bar{u}_1)^2}$$

$$r_{12} = r_{21} = \overline{(u_1 - \bar{u}_1)(u_2 - \bar{u}_2)} \qquad \text{(A-10)}$$

$$r_{13} = r_{31} = \overline{(u_1 - \bar{u}_1)(v_1 - \bar{v}_1)} \quad ,$$

et cetera.

The R matrix is completely determined once the following six relations are known:

$$\overline{(u - \bar{u})^2} = (\overline{u_1^2} - \bar{u}_1^2) - (\overline{u_2^2} - \bar{u}_2^2) + 2j(\overline{u_1 u_2} - \bar{u}_1\bar{u}_2) \qquad \text{(A-11a)}$$

$$\overline{(u - \bar{u})(u^* - \bar{u}^*)} = (\overline{u_1^2} - \bar{u}_1^2) + (\overline{u_2^2} - \bar{u}_2^2) \qquad \text{(A-11b)}$$

$$\overline{(u - \bar{u})(v - \bar{v})} = (\overline{u_1 v_1} - \bar{u}_1\bar{v}_1) - (\overline{u_2 v_2} - \bar{u}_2\bar{v}_2) + j(\overline{u_1 v_2} - \bar{u}_1\bar{v}_2)$$
$$+ j(\overline{u_2 v_1} - \bar{u}_2\bar{v}_1) \qquad \text{(A-11c)}$$

$$\overline{(u - u)(v^* - \bar{v}^*)} = (\overline{u_1 v_1} - \bar{u}_1\bar{v}_1) + (\overline{u_2 v_2} - \bar{u}_2\bar{v}_2) - j(\overline{u_1 v_2} - \bar{u}_1\bar{v}_2)$$
$$+ j(\overline{u_2 v_1} - \bar{u}_2\bar{v}_1) \qquad \text{(A-11d)}$$

$$\overline{(v - \bar{v})^2} = (\overline{v_1^2} - \bar{v}_1^2) - (\overline{v_2^2} - \bar{v}_2^2) + j(\overline{v_1 v_2} - \bar{v}_1\bar{v}_2) \qquad \text{(A-11e)}$$

$$\overline{(v - \bar{v})(v^* - \bar{v}^*)} = (\overline{v_1^2} - \bar{v}_1^2) + (\overline{v_2^2} - \bar{v}_2^2) \quad . \qquad \text{(A-11f)}$$

Note that any element of R can be obtained by taking the real or imaginary part of a sum or difference of two of the above expressions. For example,

$$r_{23} = \overline{(v_1 - \bar{v}_1)(u_2 - \bar{u}_2)} = \overline{v_1 v_2} - \bar{v}_1 \bar{u}_2$$

$$= 1/2 \ \mathrm{Im}\left\{\overline{(u - \bar{u})(v - \bar{v})} + \overline{(u - \bar{u})(v^* - \bar{v}^*)}\right\} \quad . \qquad \text{(A-12)}$$

For the averages, we have

$$\bar{u} = \overline{\int g_1(t) r(t) dt} = \int g_1(t) \overline{r(t)} dt \quad , \qquad \text{(A-13)}$$

where

$$\overline{r(t)} = \overline{[\eta + h(t)]\ e^{\psi(t)} s(t) + n(t)}$$

$$= \eta\ e^{\overline{\psi(t)}} s(t) \quad . \qquad \text{(A-14)}$$

This average is intended to be taken over a period of time that is long with respect to a bit duration T, but short with respect to the time scale of the focus component. Hence, $\psi(t)$ is a constant over the averaging period and

$$\overline{r(t)} = \eta e^{\psi(t)}\ s(t) \quad . \qquad \text{(A-15)}$$

A similar result is obtained for v.

Equations (A-11) are easily evaluated in terms of the channel correlation functions $\overline{h(t_1)h(t_2)}$ and $\overline{h(t_1)h^*(t_2)}$.

For example,

$$\overline{(u - u)^2} = \overline{\left[\int_o^T dt g_1(t)[r(t) - \eta\, e^{\psi(t)} s(t)]\right]^2}$$

$$= \int_o^T dt_1 \int_o^T dt_2\, g_1(t_1) g_1(t_2) \overline{r(t_1) r(t_2)}$$

$$- \eta^2 e^{2\psi(t)} \left[\int_o^T g_1(t) s(t)\right]^2 \quad . \tag{A-16}$$

Because $\psi(t)$ varies slowly, we have

$$\overline{r(t_1)r(t_2)} = \overline{\left\{[\eta + h(t_1)]e^{\psi(t)} s(t_1) + n(t_1)\right\}\left\{[\eta + h(t_2)]e^{\psi(t)} s(t_2) + n(t_2)\right\}}$$

$$= \left[\eta^2 + \overline{h(t_1)h(t_2)}\right] e^{[\psi(t_1) + \psi(t_2)]} s(t_1)s(t_2) + \overline{n(t_1)n(t_2)}$$

$$= e^{2\psi(t)} \left[\eta^2 + \overline{h(t_1)h(t_2)}\right] s(t_1)s(t_2) + \overline{n(t_1)n(t_2)} \quad . \tag{A-17}$$

The noise is a complex process--the real and imaginary parts of which are (1) independent, (2) zero mean, and (3) identically distributed; therefore

$$\overline{n(t_1)n(t_2)} = \overline{[x_n(t_1) + jy_n(t_1)][x_n(t_2) + jy_n(t_2)]}$$

$$= \overline{x_n(t_1)x_n(t_2)} - \overline{y_n(t_1)y_n(t_2)} = 0 \quad . \tag{A-18}$$

Hence,

$$\overline{(u - \bar{u})^2} = e^{2\psi(t)} \int_o^T dt_1 \int_o^T dt_2\, g_1(t_1) g_1(t_2) A_{hh}(t_1, t_2) s(t_1) s(t_2) \quad , \tag{A-19}$$

where $A_{hh}(t_1,t_2) = \overline{h(t_1)h(t_2)}$. The other expressions in (A-11) are determined similarly (the noise term obviously does not always cancel itself out).

The channel correlation functions are complex and given by

$$h(t_1)h(t_2) = \overline{[x(t_1) + jy(t_1)][x(t_2 + jy(t_2)]}$$

$$= \overline{x(t_1)x(t_2)} - \overline{y(t_1)y(t_2)} + j\left[\overline{x(t_1)y(t_2)} + \overline{x(t_2y(t_1)}\right] \quad \text{(A-20a)}$$

$$\overline{h(t_1)h^*(t_2)} = \overline{x(t_1)x(t_2)} + \overline{y(t_1)y(t_2)} \quad . \quad \text{(A-20b)}$$

The channel is assumed to be stationary, hence Eqs. (20a,b) are functions of only the difference $\tau = t_1 - t_2$, e.g.,

$$\overline{x(t_1)x(t_2)} = R_{xx}(\delta\tau) \quad . \quad \text{(A-21)}$$

We also assume that all channel correlation functions are Gaussian of the form

$$R(\delta\tau) = \sigma^2 e^{-\frac{\pi^2}{\ell n(2)}\left(\frac{\delta t}{\tau}\right)^2} \quad \text{(A-22)}$$

where the constant σ^2 is given by

$$\sigma_{xx}^2 = \overline{x^2(t)}$$

$$\sigma_{yy}^2 = \overline{y^2(t)}$$

$$\sigma_{xy}^2 = \rho\, \sigma_{xx}\sigma_{yy}$$

and $$\rho = \overline{x(t)y(t)} \quad .$$

This particular form is taken from Belo and Nelin (1962). We note that $B = 1/\tau$ is the half-power bandwidth of the fading channel; thus, τ is not the usual e^{-1} point of the gaussian correlation function.

DISTRIBUTION LIST

DEPARTMENT OF DEFENSE

Assistant Secretary of Defense
Comm., Cmd., Cont. & Intell.
ATTN: C3IST&CCS, M. Epstein
ATTN: Dir. of Intelligence Systems, J. Babcock

Assistant to the Secretary of Defense
Atomic Energy
ATTN: Executive Assistant

Command & Control Technical Center
ATTN: C-312, R. Mason
ATTN: C-650, G. Jones
3 cy ATTN: C-650, W. Heidig

Defense Advanced Rsch. Proj. Agency
ATTN: TIO

Defense Communications Agency
ATTN: Code 480
ATTN: Code R1033, M. Raffensperger
ATTN: Code 810, J. Barna
ATTN: Code 205
ATTN: Code 101B
ATTN: Code 480, F. Dieter

Defense Communications Engineer Center
ATTN: Code R720, J. Worthington
ATTN: Code R410, J. McLean
ATTN: Code R410, R. Craighill
ATTN: Code R123

Defense Intelligence Agency
ATTN: DB-4C, E. O'Farrell
ATTN: HO-TR, J. Stewart
ATTN: DB, A. Wise
ATTN: DT-5
ATTN: DT-1B
ATTN: DC-7D, W. Wittig

Defense Nuclear Agency
ATTN: STVL
3 cy ATTN: RAAE
4 cy ATTN: TITL

Defense Technical Information Center
12 cy ATTN: DD

Field Command
Defense Nuclear Agency
ATTN: FCPR

Field Command
Defense Nuclear Agency
Livermore Division
ATTN: FCPRL

Interservice Nuclear Weapons School
ATTN: TTV

Joint Chiefs of Staff
ATTN: C3S
ATTN: C3S, Evaluation Office

DEPARTMENT OF DEFENSE (Continued)

Joint Strat. Tgt. Planning Staff
ATTN: JLA
ATTN: JLTW-2

National Security Agency
ATTN: W-32, O. Bartlett
ATTN: R-52, J. Skillman
ATTN: B-3, F. Leonard

Undersecretary of Defense for Rsch. & Engrg.
ATTN: Strategic & Space Systems (OS)

WWMCCS System Engineering Org.
ATTN: J. Hoff

DEPARTMENT OF THE ARMY

Assistant Chief of Staff for Automation & Comm.
Department of the Army
ATTN: DAAC-ZT, P. Kenny

Atmospheric Sciences Laboratory
U.S. Army Electronics R&D Command
ATTN: DELAS-EO, F. Niles

BMD Systems Command
Department of the Army
2 cy ATTN: BMDSC-HW

Deputy Chief of Staff for Ops. & Plans
Department of the Army
ATTN: DAMO-RQC

Electronics Tech. & Devices Lab.
U.S. Army Electronics R&D Command
ATTN: DELET-ER, H. Bomke

Harry Diamond Laboratories
Department of the Army
ATTN: DELHD-I-TL, M. Weiner
ATTN: DELHD-N-P, F. Wimenitz
ATTN: DELHD-N-RB, R. Williams
ATTN: DELHD-N-P

U.S. Army Comm.-Elec. Engrg. Instal. Agency
ATTN: CCC-EMEO, W. Nair
ATTN: CCC-EMEO-PED, G. Lane
ATTN: CCC-CED-CCO, W. Neuendorf

U.S. Army Communications Command
ATTN: CC-OPS-W
ATTN: CC-OPS-WR, H. Wilson

U.S. Army Communications R&D Command
ATTN: DRDCO-COM-RY, W. Kesselman

U.S. Army Foreign Science & Tech. Ctr.
ATTN: DRXST-SD

U.S. Army Materiel Dev. & Readiness Cmd.
ATTN: DRCLDC, J. Bender

U.S. Army Nuclear & Chemical Agency
ATTN: Library

DEPARTMENT OF THE ARMY (Continued)

U.S. Army Satellite Comm. Agency
ATTN: Document Control

U.S. Army TRADOC Systems Analysis Activity
ATTN: ATAA-TCC, F. Payan, Jr.
ATTN: ATAA-TDC
ATTN: ATAA-PL

DEPARTMENT OF THE NAVY

Joint Cruise Missile Project Office
Department of the Navy
ATTN: JCM-G-70

Naval Air Development Center
ATTN: Code 6091, M. Setz

Naval Air Systems Command
ATTN: PMA 271

Naval Electronic Systems Command
ATTN: PME 106-13, T. Griffin
ATTN: PME 117-2013, G. Burnhart
ATTN: PME 117-20
ATTN: PME 117-211, B. Kruger
ATTN: Code 501A
ATTN: PME 106-4, S. Kearney
ATTN: Code 3101, T. Hughes

Naval Intelligence Support Ctr.
ATTN: NISC-50

Naval Ocean Systems Center
ATTN: Code 532, J. Bickel
ATTN: Code 5322, M. Paulson
3 cy ATTN: Code 5324, W. Moler

Naval Research Laboratory
ATTN: Code 7500, B. Wald
ATTN: Code 7550, J. Davis
ATTN: Code 6700, T. Coffey
ATTN: Code 6780, S. Ossakow

Naval Space Surveillance System
ATTN: J. Burton

Naval Surface Weapons Center
ATTN: Code F31

Naval Surface Weapons Center
ATTN: Code F-14, R. Butler

Naval Telecommunications Command
ATTN: Code 341

Office of Naval Research
ATTN: Code 420
ATTN: Code 421

Office of the Chief of Naval Operations
ATTN: OP 604C
ATTN: OP 981N
ATTN: OP 941D

Strategic Systems Project Office
Department of the Navy
ATTN: NSP-2141
ATTN: NSP-2722, F. Wimberly
ATTN: NSP-43

DEPARTMENT OF THE AIR FORCE

Aerospace Defense Command
Department of the Air Force
ATTN: DC, T. Long

Air Force Avionics Laboratory
ATTN: AAD, W. Hunt
ATTN: AAD, A. Johnson

Air Force Geophysics Laboratory
ATTN: OPR-1, J. Ulwick
ATTN: PHI, J. Buchau
ATTN: LKB, K. Champion
ATTN: OPR, A. Stair
ATTN: PHP, J. Aarons
ATTN: PHP, J. Mullen

Air Force Weapons Laboratory
Air Force Systems Command
ATTN: DYC
ATTN: SUL

Air Logistics Command
Department of the Air Force
ATTN: OO-ALC/MM, R. Blackburn

Assistant Chief of Staff
Intelligence
Department of the Air Force
ATTN: INED

Assistant Chief of Staff
Studies & Analyses
Department of the Air Force
ATTN: AF/SASC, W. Adams
ATTN: AF/SASC G. Zank

Ballistic Missile Office
Air Force Systems Command
ATTN: MNNL, S. Kennedy
ATTN: MNNH, M. Baran
ATTN: MNNH

Deputy Chief of Staff
Operations Plans and Readiness
Department of the Air Force
ATTN: AFXOKT
ATTN: AFXOXFD
ATTN: AFXOKS
ATTN: AFXOKCD

Deputy Chief of Staff
Research, Development, & Acq.
Department of the Air Force
ATTN: AFRDSS
ATTN: AFRDQ
ATTN: AFRDSP
ATTN: AFRDS

Electronic Systems Division
Department of the Air Force
ATTN: DCKC, J. Clark

Electronic Systems Division
Department of the Air Force
ATTN: XRW, J. Deas

Electronic Systems Division
Department of the Air Force
ATTN: YSEA
ATTN: YSM, J. Kobelski

DEPARTMENT OF THE AIR FORCE (Continued)

Foreign Technology Division
Air Force Systems Command
ATTN: NIIS, Library
ATTN: SDEC, A. Oakes
ATTN: TQTD, B. Ballard

Headquarters Space Division
Air Force Systems Command
ATTN: SKA, M. Clavin
ATTN: SKA, C. Rightmyer

Headquarters Space Division
Air Force Systems Command
ATTN: SZJ, W. Mercer
ATTN: SZJ, L. Doan

Rome Air Development Center
Air Force Systems Command
ATTN: TSLD
ATTN: OCS, V. Coyne

Rome Air Development Center
Air Force Systems Command
ATTN: EEP

Strategic Air Command
Department of the Air Force
ATTN: OOKSN
ATTN: XPFS
ATTN: DCXT
ATTN: DCXT, T. Jorgensen
ATTN: NRT
ATTN: DCX
ATTN: DCXF

DEPARTMENT OF ENERGY CONTRACTORS

EG&G, Inc.
Los Alamos Division
ATTN: D. Wright
ATTN: J. Colvin

Lawrence Livermore Laboratory
ATTN: Technical Information Dept. Library

Los Alamos Scientific Laboratory
ATTN: P. Keaton
ATTN: D. Westervelt
ATTN: R. Taschek

Sandia Laboratories
ATTN: Space Project Div.
ATTN: D. Dahlgren
ATTN: D. Thornbrough
ATTN: 3141
ATTN: Org. 1250, W. Brown

Sandia Laboratories
Livermore Laboratory
ATTN: T. Cook
ATTN: B. Murphey

OTHER GOVERNMENT AGENCIES

Central Intelligence Agency
ATTN: OSI/PSTD

Department of Commerce
National Bureau of Standards
ATTN: R. Moore

OTHER GOVERNMENT AGENCIES (Continued)

Department of Commerce
National Oceanic & Atmospheric Admin.
Environmental Research Laboratories
ATTN: R. Grubb

Institute for Telecommunications Sciences
National Telecommunications & Info. Admin.
ATTN: D. Crombie
ATTN: A. Jean
ATTN: L. Berry
ATTN: W. Utlaut

U.S. Coast Guard
Department of Transportation
ATTN: G-DOE-3/TP54, B. Romine

DEPARTMENT OF DEFENSE CONTRACTORS

Aerospace Corp.
ATTN: T. Salmi
ATTN: I. Garfunkel
ATTN: V. Josephson
ATTN: N. Stockwell
ATTN: R. Slaughter
ATTN: D. Olsen
ATTN: S. Bower
ATTN: F. Morse

University of Alaska
ATTN: Technical Library
ATTN: T. Davis
ATTN: N. Brown

Analytical Systems Engineering Corp.
ATTN: Radio Sciences

Analytical Systems Engineering Corp.
ATTN: Security

Barry Research Corporation
ATTN: J. McLaughlin

BDM Corp.
ATTN: L. Jacobs
ATTN: T. Neighbors

Berkeley Research Associates, Inc.
ATTN: J. Workman

Boeing Co.
ATTN: G. Hall
ATTN: S. Tashird
ATTN: M/S 42-33, J. Kennedy

University of California at San Diego
ATTN: H. Booker

Charles Stark Draper Lab., Inc.
ATTN: J. Gilmore
ATTN: D. Cox

Computer Sciences Corp.
ATTN: H. Blank

Comsat Labs.
ATTN: G. Hyde
ATTN: R. Taur

Cornell University
ATTN: D. Farley, Jr.

DEPARTMENT OF DEFENSE CONTRACTORS (Continued)

Electrospace Systems, Inc.
ATTN: H. Logston

ESL, Inc.
ATTN: J. Roberts
ATTN: C. Prettie
ATTN: J. Marshall

Ford Aerospace & Communications Corp.
ATTN: J. Mattingley

General Electric Co.
ATTN: M. Bortner

General Electric Co.
ATTN: C. Zierdt
ATTN: A. Steinmayer
ATTN: S. Lipson

General Electric Co.
ATTN: F. Reibert

General Electric Company—TEMPO
ATTN: W. Knapp
ATTN: D. Chandler
ATTN: DASIAC
ATTN: T. Stevens
ATTN: M. Stanton

General Electric Tech. Services Co., Inc.
ATTN: G. Millman

General Research Corp.
ATTN: J. Garbarino
ATTN: J. Ise, Jr.

GTE Sylvania, Inc.
ATTN: M. Cross

HSS, Inc.
ATTN: D. Hansen

IBM Corp.
ATTN: F. Ricci

University of Illinois
ATTN: K. Yeh

Institute for Defense Analyses
ATTN: J. Bengston
ATTN: E. Bauer
ATTN: H. Wolfhard
ATTN: J. Aein

International Tel. & Telegraph Corp.
ATTN: Technical Library
ATTN: G. Wetmore

JAYCOR
ATTN: S. Goldman

JAYCOR
ATTN: D. Carlos

Kaman Sciences Corp.
ATTN: T. Meagher

Linkabit Corp.
ATTN: I. Jacobs

DEPARTMENT OF DEFENSE CONTRACTORS (Continued)

Johns Hopkins University
ATTN: Document Librarian
ATTN: T. Potemra
ATTN: B. Wise
ATTN: T. Evans
ATTN: J. Newland
ATTN: P. Komiske

Litton Systems, Inc.
ATTN: R. Grasty

Lockheed Missiles & Space Co., Inc.
ATTN: W. Imhof
ATTN: R. Johnson
ATTN: M. Walt

Lockheed Missiles & Space Co., Inc.
ATTN: Dept. 60-12
ATTN: D. Churchill

M.I.T. Lincoln Lab.
ATTN: L. Loughlin
ATTN: D. Towle

McDonnell Douglas Corp.
ATTN: J. Moule
ATTN: N. Harris
ATTN: G. Mroz
ATTN: W. Olson

Meteor Communications Consultants
ATTN: R. Leader

Mission Research Corp.
ATTN: D. Sowle
ATTN: S. Gutsche
ATTN: R. Hendrick
ATTN: R. Bogusch
ATTN: F. Fajen

Mitre Corp.
ATTN: C. Callahan
ATTN: B. Adams
ATTN: A. Kymmel
ATTN: G. Harding

Mitre Corp.
ATTN: W. Hall
ATTN: W. Foster
ATTN: M. Horrocks

Pacific-Sierra Research Corp.
ATTN: E. Field, Jr.

Pennsylvania State University
ATTN: Ionospheric Research Lab.

Photometrics, Inc.
ATTN: I. Kofsky

Physical Dynamics, Inc.
ATTN: E. Fremouw

R & D Associates
ATTN: L. Delaney
ATTN: B. Yoon

DEPARTMENT OF DEFENSE CONTRACTORS (Continued)

R & D Associates
ATTN: W. Karzas
ATTN: H. Ory
ATTN: B. Gabbard
ATTN: C. MacDonald
ATTN: M. Gantsweg
ATTN: C. Greifinger
ATTN: R. Lelevier
ATTN: F. Gilmore
ATTN: W. Wright, Jr.
ATTN: R. Turco

Rand Corp.
ATTN: C. Crain
ATTN: E. Bedrozian

Riverside Research Institute
ATTN: V. Trapani

Rockwell International Corp.
ATTN: J. Kristof

Santa Fe Corp.
ATTN: E. Ortlieb

Science Applications, Inc.
ATTN: L. Linson
ATTN: J. McDougall
ATTN: D. Hamlin
ATTN: E. Straker
ATTN: D. Sachs
ATTN: C. Smith

Science Applications, Inc.
ATTN: D. Divis

DEPARTMENT OF DEFENSE CONTRACTORS (Continued)

SRI International
ATTN: G. Smith
ATTN: W. Chesnut
ATTN: W. Jaye
ATTN: D. Neilson
ATTN: R. Livingston
ATTN: R. Leadabrand
ATTN: G. Price
ATTN: A. Burns
ATTN: C. Rino
ATTN: M. Baron

Teledyne Brown Engineering
ATTN: R. Deliberis

Tri-Com, Inc.
ATTN: D. Murray

TRW Defense & Space Sys. Group
ATTN: R. Plebuch
ATTN: S. Altschuler
ATTN: D. Dee

Utah State University
ATTN: K. Baker
ATTN: L. Jensen

Visidyne, Inc.
ATTN: J. Carpenter

Science Applications, Inc.
ATTN: SZ